Catalysis Today

Design of Ni-based catalysts supported over binary La-Ce oxides: Influence of La/Ce ratio on the catalytic performances in DRM

--Manuscript Draft--

Manuscript Number:	CATTOD-D-21-00243R1
Article Type:	SI:Support role in catalysis
Keywords:	dry reforming of methane (DRM); Ni-based catalysts; La2O3-CeO2 binary oxide, solid solution.
Corresponding Author:	Leonarda Francesca Liotta, Director of Research CNR-ISMN Palermo, ITALY
First Author:	Maria Grabchenko, PhD, researcher
Order of Authors:	Maria Grabchenko, PhD, researcher
	Giuseppe Pantaleo
	Fabrizio Puleo, PhD, researcher
	Tamara Kharlamova, PhD, researcher
	V. Zaikovskii
	Olga Vodyankina, Prof.
	Leonarda Francesca Liotta, Director of Research
Manuscript Region of Origin:	ITALY
Abstract:	CeO 2 and binary La-Ce oxides, with different La/Ce atomic ratios (1:4; 1:1; 4:1), were synthesized using sol-gel method in the presence of citric acid in ammonia solution, at pH~9, and Ni (10wt%) was added by wetness impregnation method. The physical-chemical properties, catalytic activity and long-run stability of the so prepared catalysts were evaluated in DRM reaction. Characterizations of both fresh and spent catalysts were carried out using low-temperature N 2 adsorption, XRD, TGA, TPR, Raman and TEM analyses. The DRM gradient catalytic tests performed in the range of 400-800°C revealed higher catalytic conversions for Ni/La 2 O 3 -CeO 2 catalysts, especially for those with La/Ce ratio 1:4 and 1:1. The stable conversions of CH 4 and CO 2 (long run at 650 °C for 24h) registered for such Ni/La 2 O 3- CeO 2 catalysts were attributed to the presence of small Ni crystallites. During long run tests, Ni-LaCe 1:4 and Ni-LaCe 1:1 formed the same types of carbon, both as filaments and layered carbon with graphene structure, but their catalytic activity was retained. Ni/CeO 2 showed the smallest content of carbon, however, exhibited lower CH 4 and CO 2 conversions in comparison with the Ni-LaCe systems, due to the presence of big Ni particles with sizes of up to 0.5 μm.

CNR ISMN
ISTITUTO PER LO STUDIO DEI MATERIALI NANOSTRUTTURATI
SEDE DI PALERMO

Palermo, 29 June 2021

Dear Prof. Anil C. Banerjee,

Enclosed you will find the revised version of the manuscript entitled:" Design of Ni-based catalysts supported over binary La-Ce oxides: Influence of La/Ce ratio on the catalytic performances in DRM"

Authors:

M. Grabchenko, G. Pantaleo, F. Puleo, T.S. Kharlamova, V.I. Zaikovskii, O. Vodyankina*, L.F. Liotta*

All the changes done have been highlighted in red color. We are also attaching our responses to comments of reviewers.

Sincerely yours

Dr. Leonarda F. Liotta

Leonarda Liotta

DIREZIONE VIA SALARIA KM 29,300 - 00015 MONTEROTONDO STAZIONE (ROMA) ITALY
T: +39.06 90 672 484 F: +39.06 90 672 372
E: segreteria@ismn.cnr.it W: www.ismn.cnr.it
C.F.: 80054330586 P.IVA: 02118311006

BOLOGNA
Via Piero Gobetti, 101
40129 Bologna - Italy
T: +39.051 639 8513
F: +39.051 639 8540

PALERMO
Via Ugo La Malfa, 153
90146 Palermo - Italy
T: +39.091 680 9360
F: +39.091 680 9399

ROMA SAPIENZA
P.le Aldo Moro, 5
00185 Roma- Italy
T: +39.06 90 672 484
F: +39.06 90 672 372

Reviewer #1: Review

This paper presents interesting and useful results related to effect of La doping on catalytic activity and stability of Ni-loaded ceria in methane dry reforming. Applied methods and presentation of results are adequate, discussion is proper, conclusions are justified. International team of authors are known for their proper qualifications in this field with a lot of publication in the International journals. So, paper can be accepted for publication. Some minor faults in English such as unfinished phrases (page 9, lines 238-239 "According with the previous investigations of the mixed Ce1−xLaxO2−x/2 oxides [32, 34-36] the partial solubility of cerium and lanthanum oxides in each other.", etc etc) can be corrected at proofsreading stage.

Answer: These phrases have been corrected, as well as the English faults.

Reviewer #2: This manuscript titled Design of Ni-based catalysts supported over binary La-Ce oxides: Influence of La/Ce ratio on the catalytic performances in DRM fits well with the scope of the journal Catalysis Today. And well to this special issue. Prior its potential publication I suggest some improvements.

First of all, I t would be good in the Introduction to see the beneficial effects in using La or Ce as promotors/supports or so. This is not well presented. Secondly, please show better the novelty of this study.

Answer: The bifunctional action of the supports was not described in detail in the introduction part because the main focus of this work was directed to the composition and structure of the supports, in particular to limiting the segregation of individual oxides by the method of preparation and composition of the supports.

We thank the reviewers, according to the comments the introduction has been emphasized on novelty. The novelty of the work is that there is no unequivocal opinion about conditions of the Ce1-xLaxO2-δ solid solution formation and regarding of the highest degree of Ce substitution by La, depending on the preparation conditions and pre-treatment. No phase characterization was reported for mixed cerium-lanthanum oxides, Ce1-xLaxO2-x/2, with composition between x = 0.6 and x = 0.9.

We propose a preparation method of supports and a Ce/La ratio that does not lead to segregation of individual oxides, which positively affects the catalytic activity.

About the results: I suggest to replot the figures with XRD. They are very difficult to read please play with Y axis and show all the plots in separating them.

Answer: All figures with XRD were replotted (Fig.1,3,6).

About the XRD, I do not believe on the delta D/D results, the uncertainties are too small? How the authors are sure about those points. the same remark is valid for all the significant digits used please use the same numbers.

Answer: Δd/d is internal microstrain associated with variations in the d-spacing of the scattering crystals. This parameter for ideal crystal without variations in the d-spacing is tending to zero. For real crystals it can be varied from 10^{-5} to 10^{-3} (or from 10^{-3} to 10^{-1} %) [V. Yon, N. Rochat, M. Charles, E. Nolot, P. Gergaud, Phys. Status Solidi B 2020, 257, 1900579; L. Motevalizadeh, Z. Heidary, M. Ebrahimizadeh Abrishami, Bull. Mater. Sci. 2014, 37 (3) 397–405; B. Xu, M.B. Toffolo, L. Regev, E. Boaretto, K.M. Poduska, Anal. Methods, 2015, 7, 9304]. The X-ray crystal size D_{XRD} and microstrains Δd/d were calculated from broadening of peaks on XRD patterns using Williamson–Hall method. An intrinsic experimental broadening of peaks was estimated using a silicon powder standard. We corrected the Δd/d values (dimensionless quantity) limited them by 10^{-4} accuracy.

The information about the method used to calculate the X-ray crystal size D_{XRD} and microstrains Δd/d was also corrected in the Experimental section.

The crystal lattice parameter of ceria determined from the position of the peaks on the XRD pattern was limited by accuracy of 10^{-2} nm.

About DRM, it would be nice to discuss a bit the thermodynamics and the fact the at low Temp, C formation is favoured

Please add a plot in that sense in the text and discuss this point.

Answer: Some information about thermodynamics has been added to the catalytic part.

About the Figure presenting the 24 h runs, please this is impossible to read please separate conversion, yield etc... in figure a, b, c etc...

Answer: Fig.5 was changed with separation of conversions and yield.

In this section! Why some catalysts are activited and why others are deactivated ? is there any Ni redispersion ? Do you have the TEM or other characterization in which you can really compare the catalysts before and after run

Why TEM of reduced is not presented ? why XRD of spent is not presented.

Answer: All nickel catalysts were investigated at the stages: after calcination, after reduction before the catalytic test and after DRM tests by XRD and TEM methods. The XRD results of fresh, reconstituted and used samples are presented in the manuscript in Figures 1, 3 and 6, respectively. Images of TEM HR and STEM-HAADF with EDX measurements for reduced catalysts are presented in the Supporting Information (Fig. S1-S4) to not overload the main body of the article by many pictures. The interpretation of TEM data for reduced is presented in section 3.2. TEM HR images for spent catalysts are shown in Figure 9.

We observe a change in the size of nickel crystallites before and after catalysis (Table 4 and Table 5). The increase in the size of crystallites from 78 to 84 nm for Ni-Ce catalyst, from 10

to 20 nm for Ni-LaCe 1:4 and from 26 to 30 nm for Ni-LaCe 1:1 occurred due to sintering at high temperatures.

Nickel redispersion does not take place due to the absence of a redox reaction atmosphere. If you mean a decrease in the size of nickel particles due to their removal by filaments ("whiskers"), in this case yes, we observe it. However, it is difficult to estimate the size of the removed particles, while the crystallite size according to the XRD data is the average value.

Finally, please be more positive in your conclusions ! Why the Ni particle size are so big ? is there any possibility to control them during synthesis/calcination etc... ?

Answer: Big Ni particles (up to 0.5 μm) were found only for the Ni-Ce sample. The addition of La to the support composition (La/Ce atomic ratio 1:4 and 1:1) significantly decrease the sizes of Ni particles up to 20-50 nm for Ni-LaCe 1:1, 5-20 nm for Ni-LaCe 1:4 and 5-10 nm for Ni-LaCe 4:1 (TEM data). The key to control the size and nature of the nickel precursors is changing the La/Ce ratio, which affects the strength of the metal-support interaction. $Ce_{1-x}La_xO_{2-\delta}$ support with 1:4 and 1:1 of La/Ce atomic ratio provides optimal Ni dispersion for DRM.

This manuscript is very interesting and with all these minors corrections it will be very interesting for community.

Reviewer #3: The manuscript is certainly of interest for this journal but needs revision prior to its consideration for acceptance and publishing. Below please find suggestions and comments which should help the authors improve it:

(1) Graphical abstract. Some elements of the picture are very small and thus not well seen. It is recommended that the authors think how to improve their Graphical Abstract.

Answer: The Graphical Abstract has been improved. Some elements in the figure have been enlarged and made clearer. The Graphical Abstract have a high resolution, but the quality may be worse due to compression of picture in the pdf format of manuscript, which will not affect the quality of the graphical abstract in the future published article.

(2) Experimental section. It is recommended that the authors add the main equations used for calculations of conversion and yield, as some readers may not be familiar with the topic very well and thus cannot follow logic well.

Answer: The conversion of the CH_4/CO_2 and the selectivity of the products were calculated as follows:

$$CH_4 \text{ conversion } (\%) = \frac{(CH_4)_{in} - (CH_4)_{out}}{(CH_4)_{in}} 100$$

$$CO_2 \text{ conversion } (\%) = \frac{(CO_2)_{in} - (CO_2)_{out}}{(CO_2)_{in}} 100$$

$$H_2 \text{ yield } (\%) = \frac{(H_2)_{out}}{(CH_4)_{in}} \cdot \frac{100}{2}$$

$$CO \text{ yield } (\%) = \frac{CO_{in}}{(CH_4)_{in}+(CO_2)_{in}} 100$$

$$H_2 \text{ selectivity } (\%) = \frac{H_2}{2((CH_4)_{in}-(CH_4)_{out})} 100$$

$$CO \text{ selectivity } (\%) = \frac{CO}{((CH_4)_{in}+(CO_2)_{in})-((CH_4)_{out}+(CO_2)_{out})} 100$$

This information was added in experimental part.

(3) The authors used XRD to study details of the structure in their catalysts after calcination and reduction. However, they did not mention anything about any changes in the structure of the same samples, if any, after catalytic tests. This information would be helpful.

Answer: The data on crystalline phase parameters for the Ni-containing catalysts after DRM were added (Table 5) and discussed in the revised manuscript.

Specifically, the following sentences were added in the text of the revised manuscript, paragraph 3.4:

"Fig.6 shows the XRD patterns of the catalysts after DRM, with the crystalline phase parameters being presented in Table 5. According to the XRD data, the fluorite type phase and metallic Ni were detected in the Ni-Ce, Ni-LaCe1:4, and Ni-LaCe1:1 after DRM similarly to what observed for the hydrogen-reduced samples. No changes were found for the structural parameter of the fluorite type after reaction, while some increase in its crystallite size is revealed due to sintering at high temperatures (Table 4). An increase in the mean crystallite size of metallic Ni was also revealed for these catalysts. The most significant increase of the Ni crystallite size was found for the Ni-LaCe1:4, but it remains the smallest one among the Ni-Ce, Ni-LaCe1:4 and Ni-LaCe1:1 samples. The $Ce_{1-x}La_xO_{2-\delta}$ solid solution and Ni metallic phases were identified in the Ni-LaCe4:1 sample as previously reported for the hydrogen-reduced one. Moreover, the $La_2O_2CO_3$ phase was formed instead of the hexagonal La_2O_3 phase due to its interaction with CO_2. Some increase in the lattice parameter of $Ce_{1-x}La_xO_{2-\delta}$ solid solution is observed for the samples after DRM, while the crystallite size is practically unchanged. The Ni crystallite size in the Ni-LaCe4:1 sample could not be reliably determined due to overlapping of broad reflections from Ni and $Ce_{1-x}La_xO_{2-\delta}$ solid solution similarly to hydrogen-reduced sample.

In addition to the so far discussed changes, the presence of graphite-type carbon confirmed by reflection at $2\theta = 26°$ is revealed in Ni-LaCe catalysts after DRM. No graphite-type carbon is confirmed for the Ni-Ce sample. The amount of graphite-type carbon in the samples depends on the La:Ce ratio. Specifically, it is significantly lesser in the case of the Ni-LaCe 1:4 and Ni-LaCe 4:1 with respect to the sample Ni-LaCe 1:1".

(4) This reviewer believes that, for completeness and better understanding, adding DTA curves to weight loss curves in TGA of spent catalysts would be helpful (Fig.7).

Answer: DTA curves have been added to Figure 7.

(5) In Fig.5, where long-term stability (i.e. over a long-run test) is shown, the values shown along the y-axis should probably be conversion and yield. Please double check.

Answer: Fig.5 have been changed with separation of conversions and yield.

(6) In general, English is readable in the manuscript, but there are grammatical errors appearing here and there. Thus, the text must be carefully checked and polished to improve its readability.

Answer: Text of the manuscript was checked, and the grammar errors have been corrected.

Oggetto: Special Issue in Catalysis Today
Mittente: Anil Banerjee <banerjee_anil@columbusstate.edu>
Data: 05/06/2020, 00:23
A: leonardafrancesca.liotta@cnr.it
CC: "Monai, M. (Matteo)" <m.monai@uu.nl>

Dear Dr. Leonarda Liotta,

We are pleased to invite you to contribute an article for a Special Issue in *Catalysis Today* [An Elsevier open-access Journal with IF 4.888 and no APC] on the theme: Catalyst-support interactions in heterogeneous catalysis: from fundamental concepts to applications. The proposal is attached. At this point in time, we need the following information from you. Please respond asap.

1. Are you interested in submitting an article? YES/NO
2. Tentative title/theme of your article.
3. Tentative date by which you submit an article in the Journal webpage.

With Regards,

Guest Editors:

Prof. Anil C. Banerjee, Department of Chemistry, Columbus State University, Columbus, GA 31907, U.S.A. (banerjee_anil@columbusstate.edu);
Dr. Matteo Monai, Department of Inorganic Chemistry and Catalysis, Utrecht University, Utrecht, the Netherlands (m.monai@uu.nl).

Anil C. Banerjee, Ph.D
Professor, Department of Chemistry
Columbus State University
Columbus, GA 31907, USA
Office Phone:(706) 569-3030

Highlights

- La content increase results in enhance of NiO–$Ce_{1-x}La_xO_{2-\delta}$ interaction.
- $Ce_{1-x}La_xO_{2-\delta}$, x=0.25-0.5 support provides optimal Ni dispersion for DRM.
- $Ce_{1-x}La_xO_{2-\delta}$, x=0.75 leads to formation of lanthanum nickelates.
- Too small Ni NPs formed via $LaNiO_x$ reduction possess low DRM activity.

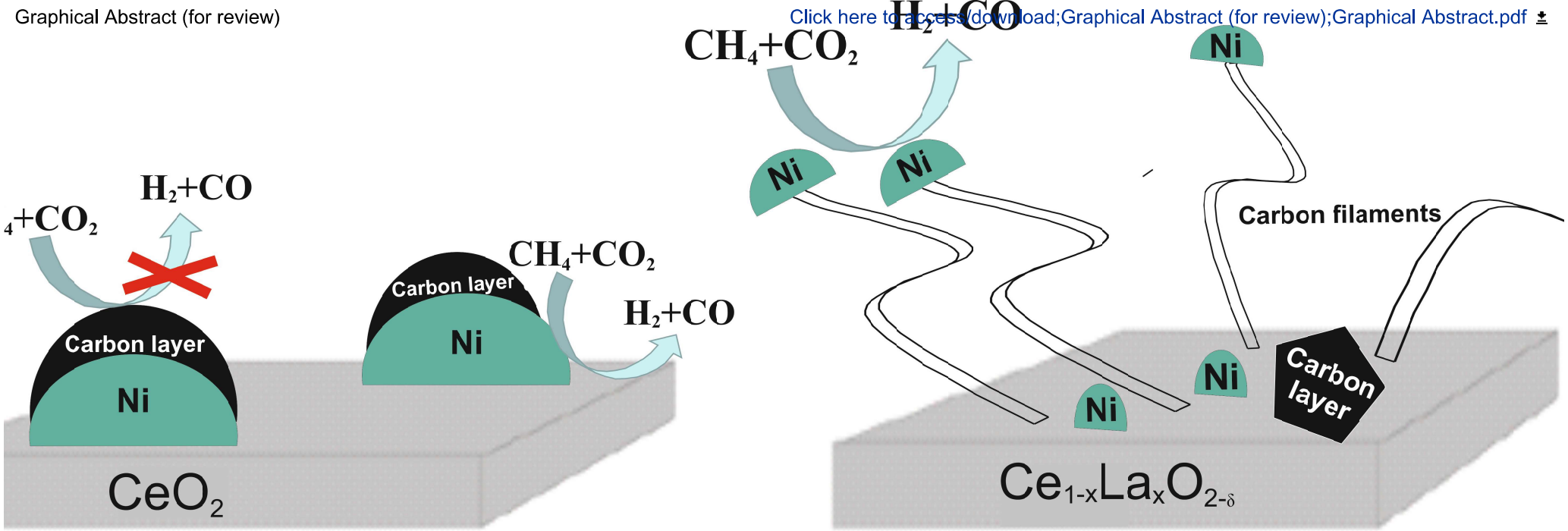

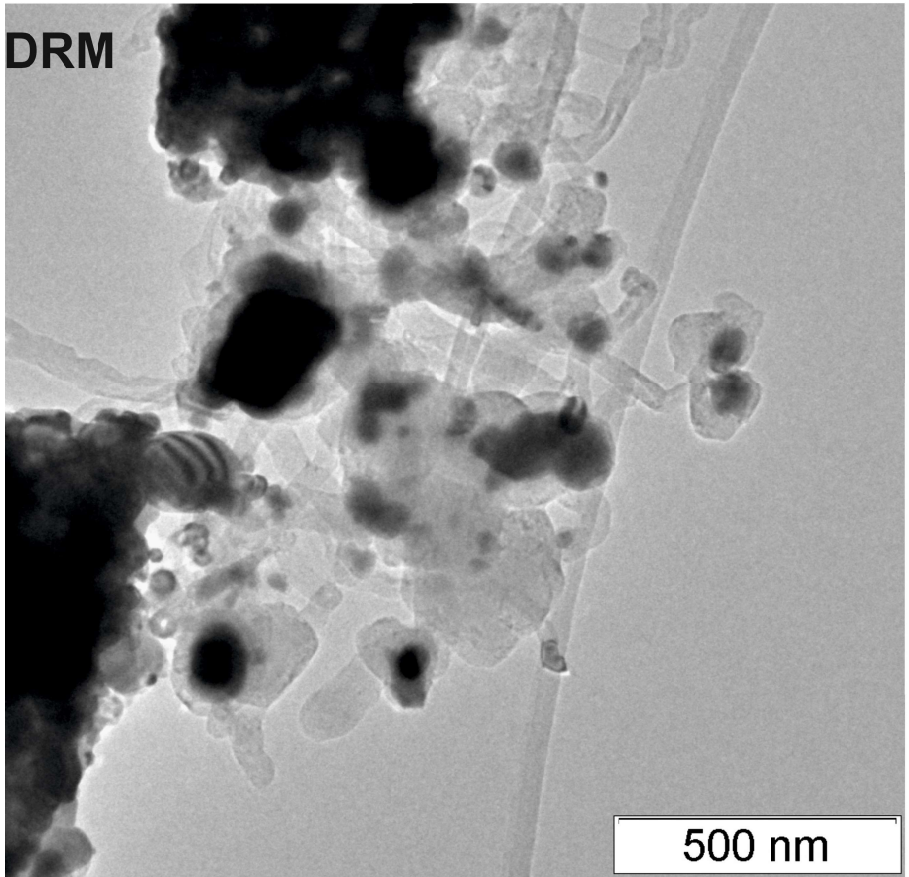

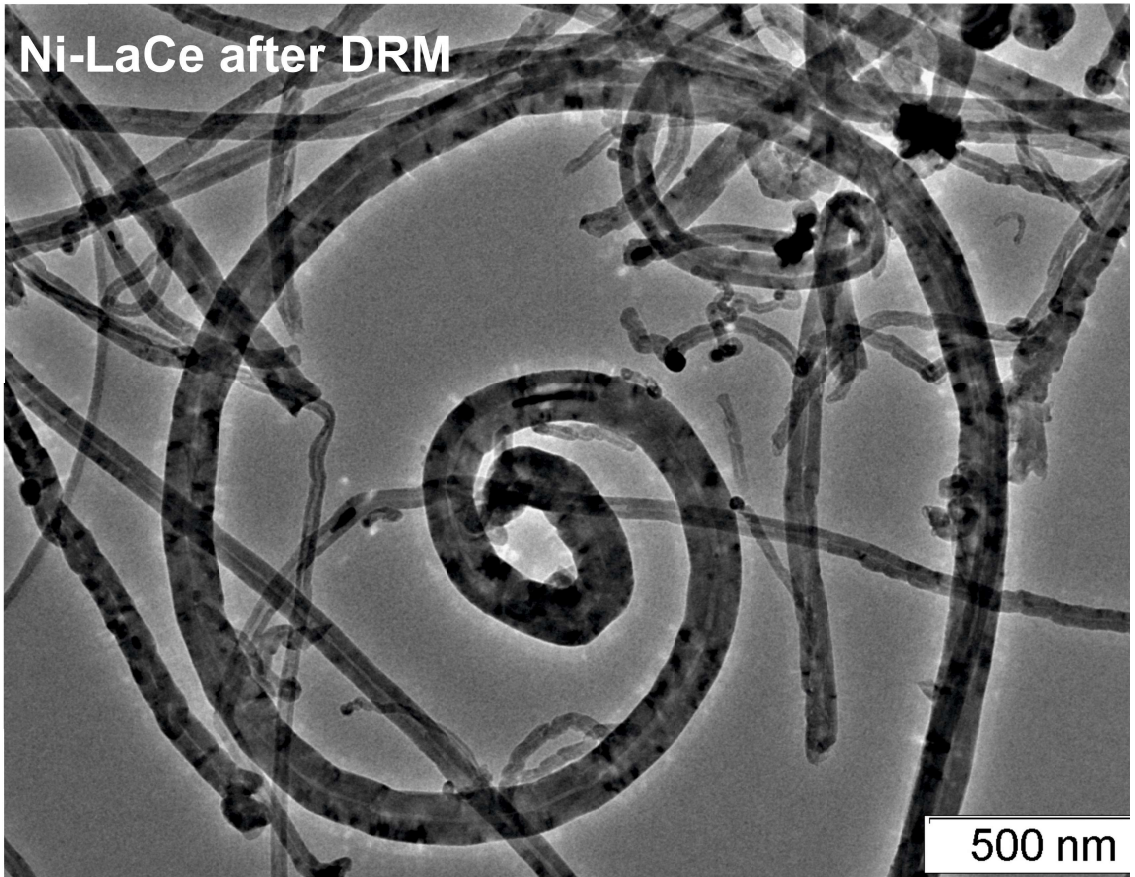

Design of Ni-based catalysts supported over binary La-Ce oxides: Influence of La/Ce ratio on the catalytic performances in DRM

M. Grabchenko[1a], G. Pantaleo[2a], F. Puleo[2], T.S. Kharlamova[1], V.I. Zaikovskii[3,4], O. Vodyankina[1*], L.F. Liotta[2*]

[1]*Tomsk State University, 36, Lenin ave., 634050 Tomsk, Russia.*

[2] *Istituto per lo Studio dei Materiali Nanostrutturati (ISMN)-CNR, via Ugo La Malfa, 153, 90146, Palermo, Italy.*

[3] *Boreskov Institute of Catalysis SB RAS, 5, Lavrentiev ave., 630090 Novosibirsk, Russia.*

[4] *Novosibirsk State University, 2, Pirogov Str., 630090 Novosibirsk, Russia.*

*Corresponding authors
Email addresses:leonardafrancesca.liotta@cnr.it (L.F.Liotta); vodyankina_o@mail.ru (O.V.Vodyankina).

[a]First authors equally contributing to the article.

Abstract

CeO_2 and binary La-Ce oxides, with different La/Ce atomic ratios (1:4; 1:1; 4:1), were synthesized using sol-gel method in the presence of citric acid in ammonia solution, at pH~9, and Ni (10wt%) was added by wetness impregnation method. The physical-chemical properties, catalytic activity and long-run stability of the so prepared catalysts were evaluated in DRM reaction. Characterizations of both fresh and spent catalysts were carried out using low-temperature N_2 adsorption, XRD, TGA, TPR, Raman and TEM analyses. The DRM gradient catalytic tests performed in the range of 400-800°C revealed higher catalytic conversions for Ni/La_2O_3-CeO_2 catalysts, especially for those with La/Ce ratio 1:4 and 1:1. The stable conversions of CH_4 and CO_2 (long run at 650 °C for 24h) registered for such Ni/La_2O_3-CeO_2 catalysts were attributed to the presence of small Ni crystallites. During long run tests, Ni-LaCe 1:4 and Ni-LaCe 1:1 formed the same types of carbon, both as filaments and layered carbon with graphene structure, but their catalytic activity was retained. Ni/CeO_2 showed the smallest content of carbon, however, exhibited lower CH_4 and CO_2 conversions in comparison with the Ni-LaCe systems, due to the presence of big Ni particles with sizes of up to 0.5 μm.

Keywords: dry reforming of methane (DRM); Ni-based catalysts; La_2O_3-CeO_2 binary oxide, solid solution.

1. Introduction

Dry reforming of methane (DRM) is considered a promising method for biomass conversion into valuable platform molecules and ecofriendly fuels via syngas formation and Fischer-Tropsch synthesis. Ni-based catalysts over high specific surface supports show the high activity in DRM [1]. However, they are characterized by low stability due to coke formation caused by the effect of acid sites of the support surface and sintering of Ni nanoparticles (NPs). Revealing and understanding the factors, determining high catalytic properties of multicomponent catalysts in biomass conversion, are an important fundamental challenge. For this reasons, Ni-based materials have been intensively studied during the last decades, with a focus on the effect of catalyst composition (oxides used as supports or additives), preparation method, and thermal treatment on the catalytic properties in DRM process [2].

As a rule, the DRM reaction is accompanied by several side reactions, with methane decomposition ($CH_4 = 2H_2 + C$), Boudouard reaction ($2CO = CO_2 + C$) and CO reduction ($CO + H_2 =$

H_2O + C) contributing to coke formation. The adsorptive decomposition of methane occurring on the nickel surface is a rate-determining step that also are accompanied the formation of carbon deposits. Due to all catalytic phenomena, occurring in the course of DRM process, it is important to understand the role of the support material [3]. Moreover, in the case of nickel catalysts, the classical requirements to the support (high surface area, mechanical stability, etc.) are expanded. The ensured maximal dispersion of metal particles, organization of strong metal–support interaction (MSI), increased Lewis basicity and the availability of the surface oxygen or hydroxyl species are the major aspects claimed to the supports featuring high catalytic performance [4,5]. A possible solution of this challenge is the use of rare earth oxides as supports that can enhance the availability of O(ads) and OH(ads) species.

Ni-containing oxides with structures of perovskite, fluorite, spinel and others complex oxides are promising precursors of nickel catalysts [2]. During the impregnation step Ni^{2+} cations enter into the oxide/hydroxide structure of the support forming solid solutions that under reducing atmosphere are destroyed forming nickel NPs. The nature of the oxide support (La_2O_3 [6], CeO_2 [7,8], MgO [9], VO_x [10], ZrO_2 [11]) influences the structure and stability of the Ni-containing precursor and those of the metallic Ni formed after reduction. Lanthanum oxide is widely used as support for DRM catalysts thanks to its double role, the stabilization of Ni NPs in a highly dispersed state and the ability to form carbonate species able to oxidize carbonaceous deposits accumulated on the surface of Ni, through the reaction $La_2O_2CO_3 + C – Ni \rightarrow La_2O_3 + 2CO + Ni$ [12].

The chemical and structural properties of the catalysts, as well as the resulting activity and stability, strongly depend on the preparation conditions.

In our previously work in Ref. [6], the experimental conditions employed in the synthesis of lanthanum oxide (citric acid with or without NH_3) were found to affect the dispersion of nickel NPs and their interaction with the support. The using of ammonia at pH~9 during the gelation step led to the formation of $La_3Ni_2O_6$ phase in the calcined sample and small Ni NPs (1–2 nm) tightly connected with La_2O_3 after reduction treatment. The catalytic results of the long run test at 650 °C during 24 h showed higher stability for the Ni/La_2O_3 catalyst prepared with ammonia in comparison with the sample synthesized without ammonia ($X(CO_2)$: 73.7% => 76.4%, $X(CH_4)$: 64.7% => 64.6%, H_2/CO: 0.77 => 0.72). The catalytic results in both, gradient and long run tests, were explained in terms of different structures and phase composition of the supports, the nature of the Ni-containing phases (NiO, $LaNiO_3$, and $La_3Ni_2O_6$) in the calcined catalysts and, consequently, sizes and interaction of Ni^0 nanoparticles with support in the reduced catalysts. Thus, using of ammonia at the preparation step is a promising tool for the design of stable Ni-containing catalyst over lanthana support.

Another promising way to increase the stability of metallic Ni NPs in Ni/La-based catalysts is by doping La_2O_3 with transition metal oxides with high oxygen mobility, namely Ce, or Zr, or Mn oxides with spinel, fluorite or perovskite structure [13-20].

Ceria is the most popular rare oxide used as support or promoter of cheaper supports due to the unique redox and acid-base properties as well as high oxygen capacity (OSC) and the ability to accumulate large number of oxygen vacancies. For that reason, Ni/CeO_2 catalysts are extensively investigated as DRM catalysts able to promote coke gasification [21-26]. Under dry reforming conditions, ceria surface can be reduced by both H_2 and CO, the latter being better reducing agent [27]. During the reaction, the bulk oxygen vacancies of CeO_2 contribute to the reduction of CO_2 to CO and adsorption of oxygen formed by CO_2 dissociation that facilitates the removal of carbon deposits [26, 28]. In addition, CeO_2 can prevent metal particles from thermal sintering due to the strong metal–support interaction [26,29,30]. The occurrence of strong metal–support interaction between Ni and CeO_2 particles can modify structural and electronic properties of Ni that impact into high activity and stability of the Ni-based catalysts [24].

Gonzalez-Delacruz et al. [26] showed that this special Ni–CeO_2 interaction is only feasible at very high temperature (at 750 °C) and is manifested in morphological changes of Ni particles (flattening of particles and decrease in the coordination number). The formation of flattened particles could explain the high stability observed under dry reforming reaction. However, despite their stability, the catalysts exhibited a low H_2/CO ratio (below 0.5) and severe carbon deposition in the form of nano-fibers for Ni loadings (7–26%) [21].

Thereby, many authors recommend the use of ceria as promoter in multicomponent catalytic system rather than as individual support for Ni catalysts. Addition of CeO_2 may enhance the surface basicity of pristine La_2O_3. The effect of surface basicity and Ni–support interaction was recently published [8]. It was shown for a $Ni/Ce_{0.85}La_{0.15}O_{2-\delta}$ sample that a proper reduction temperature (750 °C) led to an interaction between Ni and the Ce-La-O support enhancing the catalytic activity and stability. Furthermore, the authors suggested a bifunctional role of the support, where the Ce-La-O ensembles cooperated and contributed to CO_2 chemisorption and coke gasification.

The preparation of nickel catalysts based on Ce-La-O supports may be realized by impregnation of the support (La-Ce-O) with the Ni precursor or by introducing the precursor of Ni one pot during the synthesis of the support, leading to a perovskite structure ($La_{1-x}Ce_xNiO_3$). By using the citrate method for preparing catalysts with composition $La_{1-x}Ce_xNiO_3$, some authors [29, 31, 32] obtained samples which differed in both, the phase composition and the distribution of the resulting phases between the

bulk and surface of the catalysts. Someone [29] found that the solubility of cerium in the $La_{1-x}Ce_xNiO_3$ structure was limited to x <0.05; with an increase in x, the formation of individual oxide phases with a predominant distribution of CeO_2 on the surface was observed. At the same time, it was shown that mixed cerium-lanthanum oxides $Ce_{1-x}La_xO_{2-x/2}$ precipitated as bicarbonates form solid solutions in either fcc fluorite or the hexagonal phase [31, 32]. Between x = 0 and x = 0.6, the system forms solid solutions with the cubic fluorite structure. Beyond x = 0.9, it forms solid solutions with the hexagonal close-packed structure characteristic of lanthana. Lanthanum is preferentially segregated at the surface from bulk compositions up to x = 0.9, but further increments of lanthana cause the system to exhibit preferential surface segregation of the cerium moiety [31]. Moreover, it was demonstrated by the same authors [32] that lanthanum shows a marked preferential segregation to the surface of solid solutions of lanthana in ceria, while cerium preferentially segregates to the surface of solid solutions of ceria in lanthana but to a much smaller extent. The larger segregation energy of lanthanum from the ceria matrix compared to that of cerium from lanthana is due in part to its larger ionic radius. A positive effect induced by La segregation was demonstrated for a series of Ni catalysts supported on La-Ce mixed oxides with different Ni content ($Ce_{1-3x}La_{2x}Ni_xO_{2-\delta}$, x = 0.10; 0.20 and 0.25) prepared by combustion synthesis and tested in tri-reforming reaction of simulated biogas [17]. They observed that LaO_x species, coming from the support after the pre-reduction step of the catalysts, can increase the d-electron density of nickel atoms inhibiting the electron donation from the HOMO of CH_4 to d orbitals of nickel atoms, whereby suppressing the carbon deposition [17]. The highest catalytic activity was obtained with the $Ce_{0.70}La_{0.20}Ni_{0.10}O_{2-\delta}$ [17,18].

Other reports were dealing with Ni-La-Ce oxide catalysts prepared by citric method, containing Ce:La molar ratio equal to 0.55:0.45 and amount of NiO loading fixed at 12 wt% used for steam reforming of ethanol [10] or mixed oxides with composition $La_{1-x}Ce_xNiO_3$ (x = 0, 0.05, 0.4 and 0.7) tested in dry reforming of methane [29]. As shown by the authors [29], at x = 0.7 La_2O_3 is formed together with the solid solution of $La_{1-x}Ce_xNiO_3$. In both cases, the citrate complexing method allowed the formation of a lanthana-ceria solid solution providing well-dispersed Ni particles. The strong interaction between metallic Ni and the solid solution was effective in inhibiting the sintering of active phase. The catalyst with composition, $La_{0.95}Ce_{0.05}NiO_3$, was the most active as can be explained by the formation of perovskite structure with partial insertion of Ce, providing well-dispersed Ni metal, and enhancing the stability. The excellent behavior of this catalyst was explained in terms of the RWGS reaction that is favored on a Ce-enriched surface as found in the perovskite structure formed for Ce = 0.05 [29].

Although there are some reports on CeO_2-La_2O_3 systems in literature, there is no unequivocal opinion about conditions of the $Ce_{1-x}La_xO_{2-\delta}$ solid solution formation and regarding of the highest degree of Ce substitution by La, depending on the preparation conditions and pre-treatment. No phase characterization was reported for mixed cerium-lanthanum oxides, $Ce_{1-x}La_xO_{2-x/2}$, with composition between x = 0.6 and x = 0.9.

Due to the relatively low specific surface area of La-Ce solid solutions, the segregation of individual oxides of Ce and La can affect the catalytic activity, as well as the agglomeration of Ni NPs under reaction mixture at high temperatures, can be detrimental for the catalytic performances.

In this work CeO_2 and La_2O_3-CeO_2 supports have been synthesized by using a modified citrate method with addition of ammonia solution at pH ~ 9, as previously proposed by us [6]. Ni (10wt%) catalysts were prepared by wetness impregnation method. Taking into consideration the special physical-chemical properties of La-Ce solid solutions, so far reported, we have considered worth of investigation the promotion effect of CeO_2 to La_2O_3 at different La/Ce molar ratio (1:4; 1:1; 4:1), on the structural properties and catalytic performances in DRM of Ni supported catalysts prepared by the above-mentioned citrate method. The characterization of both fresh and spent catalysts was carried out using low-temperature N_2 adsorption, XRD, TGA, TPR, Raman and TEM HR analyses. The catalytic activity and stability of the prepared catalysts have been evaluated in DRM by gradient and long run modes. The activity results of Ni/La_2O_3-CeO_2 samples with different La/Ce molar ratio were compared with Ni/La_2O_3 and Ni/CeO_2 as reference catalysts.

2. Materials and Methods

2.1 Support and Catalysts preparation

CeO_2 and binary La_2O_3-CeO_2 oxides, with different La/Ce molar ratio (1:4; 1:1; 4:1), were synthesized by sol–gel method using citric acid ($C_6H_8O_7 \cdot H_2O$) as a complexing agent and ammonia (NH_4OH) as a pH agent. Analytical grade $La(NO_3)_3 \cdot 6H_2O$ and $Ce(NO_3)_3 \cdot 6H_2O$ were used as La and Ce precursors. The details of the preparation procedure have been previously reported in [6]. The resulting samples were calcined (heating ramp of 5°C $\cdot min^{-1}$) at 350 °C for 1 h and then at 800 °C for 4 h.

The Ni (10%wt) catalysts supported on the so prepared oxides were synthesized by wetness impregnation using $Ni(NO_3)_2$ $6H_2O$ as a nickel precursor. The powders after the impregnation were dried and then calcined at 600 °C for 2 h. The resultant catalysts are labeled as Ni-Ce, Ni-LaCe 1:1, Ni-LaCe 1:4 and Ni-LaCe 4:1.

173 *2.2 Catalysts characterization*

174 Elemental analysis of the catalysts was carried out by inductively coupled plasma optical emission
175 spectroscopy (ICP-OES), using HORIBA Jobin Yvon Activa instrument. The catalysts were pretreated
176 in acidic solution with H_2SO_4 and HNO_3 at 250 °C for complete dissolution. The real loading of Ni, La
177 and Ce in the prepared catalysts was equal to the nominal one ±10%.

178 The XRD measurements of the calcined/reduced and spent samples of Ni-containing catalysts
179 were carried out with a Bruker D 5000 diffractometer equipped with a Cu Kα anode in the range from
180 20 to 60º (2θ). The crystalline phase composition was established by using the JCPDS and ICSD
181 database. POWDER CELL 2.5 software package was used for determination crystal cell indexing starting
182 from powder diffraction data with Lorentz simulation. An intrinsic experimental broadening of peaks
183 was estimated using a silicon powder standard. The X-ray crystal size D_{XRD} and microstrains were
184 calculated using Williamson–Hall method.

185 Specific surface area and pore size distribution of the samples were determined by N_2 adsorption-
186 desorption isotherms at -196 °C using Carlo Erba. The specific surface area was calculated using the
187 Brunauer–Emmett–Teller (S_{BET}) method and the pore size distribution curves and pore volume were
188 determined by the Barrett–Joyner–Halenda (BJH) method from the desorption branches of the isotherms.

189 The catalysts were studied by temperature-programmed reduction (H_2-TPR) using Micromeritics
190 Autochem 2950 HP apparatus equipped with a thermal conductivity detector (TCD). The H_2-TPR
191 profiles were registered after pre-treatment of the catalysts in the temperature-programmed oxidation
192 (TPO) mode in O_2/He flow from room temperature to up to 350 °C with holding for 30 min. Then the
193 samples were cooled down up to RT. The H_2-TPR analysis was carried out in the temperature range of
194 25 - 1000 °C with a 10 °C/min heating rate. A flow rate of 5 vol. % of H_2 in Ar was 30 ml/min.

195 The morphologies of the reduced and the spent catalysts were analysed by transmission electronic
196 microscopy (TEM) using a JEM–2200FS microscope (JEOL, Japan) with an accelerating voltage of 200
197 kV. High-resolution transmission electron microscopy (HRTEM) and high-angle annular dark-field
198 scanning transmission electron microscopy (HAADF-STEM) were used. The crystal lattice parameters
199 were calculated by Fourier transform using the DigMicrograph (GATAN) software.

200 The TGA experiments were carried out with a TGA/DSC1 STAR system (Mettler Toledo) under
201 air or N_2 flow by heating from 100 to up to 1000 °C in order to evaluate the amount of carbon or
202 carbonates species deposited on Ni catalysts at the end of the DRM tests. The CO_2 evolution occurring
203 during the TGA experiments was monitored by QM analyser (Balzers. Quadstar).

Raman spectra were recorded to understand the graphitic degree of coke on the spent catalysts. Raman spectra were registered at ambient condition using InVia confocal Raman microscope (Renishaw, UK) equipped with a Leica microscope with a 50x objective. Excitation was performed with a solid-state Nd: YAG laser at a wavelength of 532 nm and a radiation power of 100 mW. To prevent heating of the sample, only 5% laser power and 50% defocusing were used. Raman spectra were measured in a spectral resolution of 2 cm^{-1}.

2.3 Catalytic test

The activity tests were carried out in a U-shaped fix-bed reactor with an inner diameter of 12 mm in an electrically heated furnace. Before the reaction, the catalyst (50 mg) was pre-treated with 5 vol%O_2/He at 350 °C during 30 min. Then the sample was reduced with 5 vol. %H_2/Ar from room temperature to up to 600 °C (heating rate 10°C $\cdot min^{-1}$) for 1 h.

The reagent gas mixture consisting of 15vol. % CH_4 + 15 vol% CO_2 in N_2 was flowed over the catalyst with a flow rate of 50 ml/min. The gradient temperature DRM tests were carried out by increasing the temperature from 400 °C to up to 800 °C (by steps of 50 °C, holding time was 30 min at a target temperature). After the catalytic run in the temperature range of 400–800 °C, the catalyst was left under the reaction mixture at 650 °C for 24 h in order to study the stability over time (long-run tests). The conversion of the CH_4/CO_2 and the selectivity of the products were calculated as follows:

$$CH_4 \text{ conversion } (\%) = \frac{(CH_4)_{in} - (CH_4)_{\text{out}}}{(CH_4)_{in}} 100;$$

$$CO_2 \text{ conversion } (\%) = \frac{(CO_2)_{in} - (CO_2)_{out}}{(CO_2)_{in}} 100;$$

$$H_2 \text{ yield } (\%) = \frac{(H_2)_{\text{out}}}{(CH_4)_{in}} \cdot \frac{100}{2};$$

$$CO \text{ yield } (\%) = \frac{CO_{in}}{(CH_4)_{in} + (CO_2)_{in}} 100;$$

$$H_2 \text{ selectivity } (\%) = \frac{H_2}{2((CH_4)_{in} - (CH_4)_{\text{out}})} 100;$$

$$CO \text{ selectivity } (\%) = \frac{CO}{((CH_4)_{in} + (CO_2)_{\text{in}}) - ((CH_4)_{out} + (CO_2)_{\text{out}})} 100.$$

3. Results and discussion

3.1 Characterization of calcined supports and catalysts

3.1.1 XRD and BET analysis

Fig.1 a displays the XRD patterns of the supports calcined at 800 °C. Pure CeO_2 exhibits well-defined peaks characteristic of the fluorite type cubic structure (space groupFm3hm, ICSD # 34394) with a lattice parameter of α=5.41 Å. All the diffractograms of the binary La-Ce oxides show a significant shift of main reflections of the fluorite type phase towards lower angles with the increase of lanthanum content. No additional reflections were observed in the patterns of the LaCe 1:4 and LaCe 1:1 supports. This finding suggests the partial substitution of Ce^{4+} (ionic radius (i.r.) = 0.111 nm for coordination number (CN) = 8 [31]) by the larger La^{3+} (i.r. = 0.130 nm for CN = 8) ion with formation of a $Ce_{1-x}La_xO_{2-\delta}$ solid solution of the cubic structure (F-type). The lattice parameter *a* and corresponding composition of the fluorite type solid solution evaluated via Vegard's law are presented in Table 1. The compositions evaluated for the LaCe 1:4 and LaCe 1:1 supports are very close to the target one of the samples. For the LaCe 4:1 support, the shift of fluorite reflections due to substitution of Ce^{4+} by La^{3+} to low angles accompanied by the appearance of the additional small peaks specifically at 2θ=37.5°, 46.5°, 48.8°, 56.8°, 58.9°, which are not attributed to the reflections from lanthanum-related phases. The appearance of additional peaks in the pattern is associated with the superstructure ordering in the $Ce_{1-x}La_xO_{2-\delta}$ fluorite type phase (S.G. Fm3hm) due to increase of oxygen vacancy concentration and formation of related C-type phase (S.G. Ia3) [32]. The lattice parameter *a* for the C-type phase is presented in Table 1, but composition of this phase was not evaluated due to deviation from Vegard's rule [33]. The full profile refinement for the single C-type phase using Ce_2O_3 (S.G. Ia3) as a model was not adequate to fit the pattern because of anomalous peak broadening and redistribution of small peak intensities. The latter can be caused by presence of defects in the structure of the C-type phase, but also by the presence of impurities of X-ray amorphous phases.

Previous investigations on mixed $Ce_{1-x}La_xO_{2-x/2}$ oxides [32, 34-36] have highlighted the partial solubility of cerium and lanthanum oxides in each other. Specifically, the solubility of lanthanum oxide in CeO_2 fluorite type phase to form $Ce_{1-x}La_xO_{2-x/2}$ solid solution is limited by ionic fraction $x \geq 0.6$, while the solubility of cerium oxide in La_2O_3 hexagonal A-type phase (S.G. $P\bar{3}m1$) is limited by $x \geq 0.9$. For compositions with x between 0.6 and 0.9, the biphasic mixtures of fluorite and A-type phases are formed. The formation of related C-type phase (S.G. Ia3) together with or instead of fluorite type phase was also indicated for non-single-phase compositions with $x > 0.6$ [32]. However, in the current LaCe 4:1 sample with the highest lanthanum content (LaCe 4:1), the primarily formation of $La_{2-x}Ce_{2x}O_{3-\delta}$ solid solution with C-type structure was observed, with no segregation of La_2O_3 or $La(OH)_3$ phases being confirmed. This C-type solid solution seems to be metastable intermediate phase preceding segregation of hexagonal La_2O_3 phase. Thus, an important result coming from this investigation is that the ammonia

addition during the preparation with citric acid of the binary LaCe oxides can promote the formation of a single-phase $La_{2-x}Ce_{2x}O_{3-\delta}$ solid solution even at high lanthanum concentration.

The analysis of the XRD peaks broadening using size-strain plot method indicates the presence of pure ceria characterized by rather large mean crystallite size of 55 nm due to sintering and relatively low microstrain (Table 1). The Ce^{4+} substitution with La^{3+} hinders crystallite growth for $Ce_{1-x}La_xO_{2-\delta}$ solid solutions (within 24–27 nm), but it results in microstrain increase due to oxygen vacancies formation in $Ce_{1-x}La_xO_{2-\delta}$ solid solutions.

In Fig.1b the diffraction patterns of the calcined Ni-containing catalysts are also displayed, with the corresponding structural and size/strain data being presented in Table 2. In the Ni-Ce catalyst, the structure and dispersion of the ceria support remains unchanged and the formation of a well crystallized NiO phase (PDF #73-1519) with the mean crystallite size of 65 nm occurs (Table 2). In Ni-LaCe 1:4 and Ni-LaCe 1:1 catalysts, a decrease of the lattice parameter of the fluorite phase as compared with the corresponding support was observed (Table 2), indicating incorporation of some Ni^{n+} ions (i.r. = 0.083 nm for n = 2, CN = 6; i.r. = 0.070 nm for n = 3, CN = 6; i.r. = 0.062 nm for n = 4, CN = 6) in the fluorite structure to form $Ce_{1-x-y}La_xNi_yO_{2-\delta}$ solid solution. Besides, in contrast to the Ni-Ce catalyst, the formation of dispersed NiO phase characterized by the mean crystallite size of ~14 nm is observed for Ni-LaCe 1:4 and Ni-LaCe 1:1 catalyst. Finally, in the Ni-LaCe 4:1 catalyst, a cubic phase of $Ce_{1-x}La_xO_{2-\delta}$ solid solution remains the main phase, but the primarily formation of dispersed $LaNiO_3$ and La_2NiO_4 phases occurs instead of NiO phase.

The full profile refinement of the pattern was not adequate because of anomalous peak broadening. So, it is not possible to say the symmetry of the cubic phase of $Ce_{1-x}La_xO_{2-\delta}$ present as well as exclude the formation of some NiO phase. Anyway, the lattice parameter of the $Ce_{1-x}La_xO_{2-\delta}$ phase is lower for the Ni-LaCe 4:1 catalyst as compared with the corresponding support. This can be due to both, the incorporation of some Ni^{n+} ions in the structure of the $Ce_{1-x}La_xO_{2-\delta}$ phase and lanthanum segregation to form $LaNiO_3$ phase. In general, the observed changes in sample composition with increase of La content indicate the increase of interaction between $Ce_{1-x}La_xO_{2-\delta}$ support and NiO (or its precursor).

Textural characteristics of the Ni-LaCe catalysts are listed in Table S1. All the samples show specific surface area values ranging from 10.8 to 13.1 m^2/g, pore volume around 0.05-0.08 cm^3/g and average pore size between ~9 and 15 nm.

3.1.2 H_2-TPR analysis

Fig. 3 presents the results of the H_2-TPR study in the order to determine the reducibility of Ni precursors on the surface of mono- and binary Ce-La oxide supports and the interaction between active components and the support surface. Table 3 summarizes the H_2 consumption values and the reduction temperatures.

The H_2-TPR profile of the Ni-Ce catalyst contains two main reduction peaks: a low-temperature peak with a maximum at 327 °C and a shoulder in the range 450-480 °C and a high-temperature consumption at 850 °C. The first reduction peak corresponds to the reduction of NiO NPs with partial reduction of the CeO_2 surface [7]. The high temperature peak, which is shifted to the lower temperature in comparison with pure CeO_2, corresponds to more easy reduction of bulk CeO_2 due to the presence of Ni^0 NPs, which are able to promote the faster reduction of CeO_2 [12, 37].

The introduction of La_2O_3 into the composition of the supports influences the shape of the H_2-TPR profiles registered for the Ni-calcined catalyst precursors. The high temperature peak above 850 °C practically disappeared for all Ni-LaCe catalysts in comparison with the Ni-CeO_2 sample, while the low-temperature peak shifted to slightly higher values (350-392 °C).

The reduction profiles of Ni-LaCe 1:4, Ni-LaCe 1:1 and Ni-LaCe 4:1 contain, in all cases, a main reduction peak in the range ~250-480 °C, centred at around 392 or at ~350 °C, respectively, which can be associated with the simultaneous reduction of NiO particles and the solid solutions $Ce_{1-x-y}La_xNi_yO_{2-\delta}$ [17]. Small peaks below 300 °C (at 180 and 260 °C) were detected only for Ni-LaCe 1:1 sample and correspond to the reduction of big NiO particles weakly interacting with the support surface. For the Ni-LaCe 4:1 sample a second peak at 520 ° C was also observed, likely due to the reduction of NiO species strongly interacting with the support along with to the reduction of some segregated ceria [38].

The investigation by H_2-TPR technique showed that the addition of CeO_2 to La_2O_3 with different of La/Ce molar ratio affects the nature of the Ni-containing phases and their interaction with the support. The interaction between NiO NPs and the surface of Ce-La seems different as a function of the composition. The weakest interaction was registered for the Ni-Ce catalyst showing the low-temperature reduction peak at the lowest temperature, 327 °C. The hydrogen consumption associated to such peak accounts for the overall reduction of Ni^{2+} to metallic Ni (experimental value 40.1 mL/g *vs* theoretical one 41.7 mL/g), but it should correspond also to a partial reduction of ionic nickel into the metallic state along with to the reduction of surface ceria (see Table 3). The peak at 850 °C is due to the reduction of ceria bulk [38]. As reported in the literature [39], the classical temperature-programmed reduction technique using a thermally controlled detector and a water vapour trap did not permit the quantification of the extent of reduction of unsupported ceria that, anyway, cannot reach full reduction, working at

atmospheric pressure. Accordingly, the experimental hydrogen consumption associated to the bulk reduction of ceria (23.1 mL/g) is significantly lower than the theoretical value (63.9 mL/g).

Looking at the temperature of the main reduction peak of Ni-LaCe binary systems, a shift toward higher temperatures was observed, especially for the Ni-LaCe 1:4, suggesting the enhanced metal-support interaction. The H_2 consumption values listed in Table 3, indicates a slight increase of the peak in the low-temperature region, in the following order: Ni-LaCe 1:1 < Ni-LaCe 4:1 < Ni-LaCe 1:4. This trend may suggest different reducibility of $Ce_{1-x-y}La_xNi_yO_{2-\delta}$ and Ni phases detected by XRD and listed in Table 2. In all cases, the experimental hydrogen values (ranging between 42.5-48 mL/g) are much lower than the theoretical ones (between ~55-68.5 mL/g) expected for the overall reduction of Ce and Ni containing phases, thus, indicating low reducibility of such species or the presence of $Ce_{1-x-y}La_xNi_yO_{2-\delta}$ phases with high Ce^{3+} content.

3.2 Characterization of reduced catalysts

In order to investigate the samples structure and morphology before DRM tests, the reduced catalysts were studied by XRD and TEM HR techniques.

Fig. 3 shows the XRD patterns of catalysts after reduction treatment at 600 °C in 5 vol. % H_2/Ar flow. The XRD pattern of reduced Ni-Ce catalyst is characterized by narrow reflections of CeO_2 fluorite type phase and metallic Ni (ICSD #4-850), suggesting the presence of large crystallites. According to the size-strain plot method (Table 4), the mean crystallite size of fluorite phase is ~60 nm and Ni is ~80 nm for Ni-Ce catalyst.

For the Ni-LaCe 1:4 and Ni-LaCe 1:1 catalysts, the structure of fluorite type solid solution was retained after the reduction treatment, with the lattice parameter was little changing due to some variations in composition. Besides, in contrast to the Ni-Ce catalyst, the diffraction peaks corresponding to Ni are broad for the Ni-LaCe 1:4 and Ni-LaCe 1:1 samples suggesting the presence of dispersed nickel species. The corresponding mean crystallite size of Ni is ~10 and ~30 nm for the Ni-LaCe 1:4 and Ni-LaCe 1:1, respectively.

For reduced Ni-LaCe 4:1 catalyst, the presence of La_2O_3 hexagonal phase and Ni cubic phase along with the cubic phase of $Ce_{1-x}La_xO_{2-\delta}$ solid solution (presumably C-phase) were found. Unfortunately, the crystallite size of Ni phase could not be reliably determined from XRD data due to overlapping of broad reflections from Ni and $Ce_{1-x}La_xO_{2-\delta}$ solid solution. However, the reflection broadening indicates that it should be rather small. The observed decrease of the lattice parameter of the cubic phase from 5.74/11.50 Å to 5.65/11.29 Å indicates the further changing in the solid solution

composition due to the sample reduction. The presence of La_2O_3 hexagonal phase in the reduced sample can be coursed by the reduction of $LaNiO_3$ and La_2NiO_4 phases as well as by additional segregation from $Ce_{1-x}La_xO_{2-\delta}$ solid solution.

In general, it can be concluded that strong interaction between support and nickel oxide species in air-reduced samples results in higher dispersion of nickel species in the reduced catalysts.

TEM HR analysis and STEM-HAADF with EDX measurements were performed in order to characterize the elemental distribution in the catalysts and to estimate the Ni particle size. From the EDX spectrum obtained from different areas of the samples, the elemental ratios of Ni, La, Ce and O were determined, and the obtained data good agreed with the composition of the samples (as derived by ICP-OES analysis).

Fig. S1 displays the HAADF image of the reduced Ni-Ce sample with the corresponding Ce and Ni mapping distribution. The obtained results suggest the existence of two types of metallic Ni particles: large Ni particles with sizes of 50–70 nm, as well as small aggregates of Ni particles with sizes of ~ 5 nm on the surface of big CeO_2 crystals (100-200 nm) (Fig.S1 b).

EDX mapping of the Ni-LaCe 1:4 sample (Fig. S2) illustrates the segregation of Ni NPs with sizes of 5–20 nm with a discrete distribution over the La-Ce-O_x surface. Moreover, for this sample, there is a uniform distribution of Ni NPs with mainly size of 5 nm, which almost completely cover the surface of the La-Ce-O_x support.

TEM and TEM HR images of the reduced Ni-LaCe 1:1 sample showed high defectiveness of structure (Fig.S3 a,b). This morphology can be connected with decomposition, under reductive atmosphere, of the ternary Ni-La-Ce-O solid solution, detected by the XRD data for the calcined sample, and formation of defective La-Ce-O_x solid solution with sizes of 1-10 nm. In Fig.S3 c several metallic Ni^0 NPs aggregated over the sample surface were detected. In details, the LaCe 1:1 support appeared irregularly coated by nickel aggregates with different sizes, ranging from 20-50 nm and between 60-90 nm.

The morphology of the reduced Ni-LaCe 4:1 sample is displayed in Fig. S4 a. The sample was presented by the domain structure. From TEM image (Fig. S4 a) it can be seen that Ni-LaCe 4:1sample has an inhomogeneous multiphase structure, while for catalysts based on another binary oxides it was shown only Ni distribution over La-Ce-O_x surface. The HAADF image of Ni-LaCe 4:1 catalyst (b) with corresponding Ni mapping distribution from selected area (c) shown the distribution of Ni particles with sizes of 5-10 nm. Moreover, it appears that the smallest nickel particles are located on the areas of support with the smallest thickness, while on the areas of the support with larger thickness the sizes of nickel

particles are larger, suggesting an agglomeration of such particles. The obtained TEM data are in good agreement with the XRD results.

3.3. Catalytic properties in DRM

The DRM catalytic tests at gradient temperature were performed between 400 °C to 800 °C. In Fig. 4 the CH_4/CO_2 conversion curves, H_2 yield and H_2/CO molar ratio are displayed for all catalysts. Table S2 summarizes the main catalytic results.

Based on the catalytic data the addition of lanthanum to ceria leads to an increase in both methane and carbon dioxide conversions. The 50%-conversion of CO_2 for Ni/Ce was observed at 650 ºC, while for Ni-LaCe 1:4, Ni-LaCe 1:1 the same conversion value was achieved at already 605 and 610 ºC, respectively. The same trend of CH_4 conversion was observed for the above samples. However, with a further increase in the La_2O_3 content in the support composition in case of Ni-LaCe 4:1 catalyst the CO_2 and CH_4 conversions were lower in comparison with the ones for Ni-Ce catalyst in the temperature range of 400 - 680 ºC. At temperature above 680 ºC the CH_4/CO_2 conversions suddenly increased for Ni-LaCe 4:1 catalyst. In addition, the Ni catalysts supported on La-Ce mixed oxide show remarkably higher H_2/CO ratio starting from 450 °C in comparison to the one supported on pure ceria (Ni/CeO_2) with values being quite close to the equilibrium. The increased content of CO in the reaction products can be associated with the implementation of side reactions, such as the reverse water-gas shift reaction ($CO_2 + H_2 \rightarrow CO + H_2O$) and the oxidation of surface carbon according to reverse Boudouard reaction ($C + CO_2 \rightarrow 2CO$). The accumulation of carbon on the surface of catalysts in the process of DRM at temperatures above 600 ° C is mainly associated with the decomposition of methane ($CH_4 \rightarrow C + 2H_2$). It should be noted that the carbon formed in this process is more reactive than the carbon that is formed in the Boudouard reaction (at temperature below 600 ° C), therefore it can be easily oxidized in the presence of CO_2 to form CO.

Stability tests were carried out in the order to investigate the performance of the catalysts during the long-time test. Fig. 5 presents the results of the DRM long run test performed at 650 °C during 24h in terms of CH_4 and CO_2 conversions and H_2 yield. The catalytic results of long-run (LR) tests were compared with data recorded during the gradient temperature tests (Table S2). The Ni-LaCe 4:1 has lowest both initial and end of conversions of CH_4 and CO_2 than other catalysts based on perovskite solid solution supports. Despite the high values of the CH_4 conversion obtained for the Ni-La, its stable decrease (by more than 5 rel. %) is observed during the entire long-run test. For the Ni catalysts prepared over La-Ce supports, the methane conversion values are slightly lower (~ 8 rel. %). However, during the

entire experiment, the high stability in terms of methane and CO_2 conversion rates for Ni-LaCe 1:4 and Ni-LaCe 1: 1 samples should be noted (Fig.5).

Thus, the addition of CeO_2 to La_2O_3 in an amount of La/Ce equal to 1:4 and 1:1 makes possible to obtain catalysts with high stability under the conditions of DRM and they are not inferior in catalytic properties to Ni-La catalyst at temperatures more than 650 ^oC, based on our previous results [6].

3.4 Study of the spent catalysts after long run tests

In order to get insights into the phenomena occurring during the DRM tests the spent catalysts studied after long-run test were analysed by several techniques. Fig.6 shows the XRD patterns of the catalysts after DRM, with the crystalline phase parameters being presented in Table 5. According to the XRD data, the fluorite type phase and metallic Ni were detected in the Ni-Ce, Ni-LaCe1:4, and Ni-LaCe1:1 after DRM similarly to what observed for the hydrogen-reduced samples. No changes of the structural parameter of the fluorite type were found after reaction, while some increase in the crystallite size is revealed due to sintering at high temperatures (Table 4). An increase in the mean crystallite size of metallic Ni was also revealed for these catalysts. The most significant increase of the Ni crystallite size was found for the Ni-LaCe1:4, but it remains the smallest one among the Ni-Ce, Ni-LaCe1:4 and Ni-LaCe1:1 samples.

The $Ce_{1-x}La_xO_{2-\delta}$ solid solution and Ni metallic phases were identified in the Ni-LaCe4:1 sample as previously reported for the hydrogen-reduced one. Moreover, the $La_2O_2CO_3$ phase was formed instead of the hexagonal La_2O_3 phase due to its interaction with CO_2. Some increase in the lattice parameter of $Ce_{1-x}La_xO_{2-\delta}$ solid solution is observed for the samples after DRM, while the crystallite size is practically unchanged. The Ni crystallite size in the Ni-LaCe4:1 sample could not be reliably determined due to overlapping of broad reflections from Ni and $Ce_{1-x}La_xO_{2-\delta}$ solid solution similarly to hydrogen-reduced sample.

In addition to the so far discussed structural changes, the presence of graphite-type carbon confirmed by reflection at $2\theta = 26°$ is revealed in Ni-LaCe catalysts after DRM. No graphite-type carbon is confirmed for the Ni-Ce sample. The amount of graphite-type carbon in the samples depends on the La:Ce ratio. Specifically, it is significantly lesser in the case of the Ni-LaCe 1:4 and Ni-LaCe 4:1 with respect to the sample Ni-LaCe 1:1.

Fig. 7 shows the data of TG analysis of the catalysts after the long run test in flow of air. Under air atmosphere, the TGA curve of the spent Ni-Ce shows slightly smaller contents of CO_2 and coke in comparison with spent catalysts prepared over binary La-Ce supports.

The registered TG profiles of Ni-LaCe differ in the position of the edge of the weight loss curve. It can be seen that for the Ni-LaCe 4:1 sample, the inflection point of the weight loss profile corresponds to a temperature of 640 ° C, and for two other Ni catalysts based on La-Ce-O, the inflection point temperature corresponds to 543 ° C and 624 ° C for Ni-LaCe 1:4 and Ni-LaCe 1:1, respectively. For the Ni-LaCe 1: 4 sample, the weight loss is ~ 30% rel., which is slightly higher compared to the Ni-LaCe 4:1 sample (~ 21%), but the temperature of the inflection point is shifted towards lower temperatures by ~100 ^{o}C. From this data it can be conclude that the formed carbon-containing deposits on the surface of the Ni-LaCe 1:4 sample are differed significantly in nature from the carbon deposited on the surface of the Ni-LaCe 4:1, that confirmed by XRD data. Thus, the composition of the support has a significant effect on the reactivity of Ni nanoparticles in the formation of carbonaceous deposits.

Raman spectroscopy was used to study the nature of the carbon deposits formed onto the spent catalysts after DRM. The peaks at 1309 cm^{-1} and 1603 cm^{-1} corresponds to a Raman-allowed phonon modes E_{2g} and involves out of phase of intra-layer displacement in the graphene structure (D band) and polycrystalline imperfect graphite (G-band), respectively. The intense peak at ~2612 cm^{-1} (2D) is typically found in graphite spectra. The relative intensity between the two peaks (I_D/I_G) may give information about the nature of carbon nanotubes and about the degree of crystallinity of the carbon formed. Smaller I_D/I_G values indicate higher crystallinity due to higher contribution of the graphitized carbon [40,41]. The calculated I_D/I_G ratio increased in the order: 1.23 (Ni-LaCe 1:1) < 1.39 (Ni-LaCe 4:1) <2.22 (Ni-LaCe 1:4) ~2.23 (Ni-Ce). Thus, crystalline carbon is formed over Ni-LaCe 1:1 and Ni-LaCe 4:1 spent samples, while amorphous carbon deposits were found predominantly over Ni-LaCe 1:4 and Ni-Ce samples.

By HR TEM the morphology of the obtained carbon deposits and their distribution over La-Ce support were studied. For the Ni-Ce spent catalyst a small amount of carbon was observed, which is formed as amorphous layers over nickel particles (thickness is 50 nm), while ceria surface is not carbonized (Fig.9a). Fig. 9 b illustrates the morphology of the carbon formed on the surface of Ni-LaCe 1:4, which is similar to Ni-Ce morphology, with addition few amount of carbon as filaments. The Ni-LaCe 1:1 and Ni-LaCe 4:1 spent sample have both as filaments and layered carbon with graphene structure (Fig.9 c, d). For Ni-LaCe 1:1 sample consisted of carbon fibers with La-Ce aggregate at the tip of filaments and capsules (Fig.9 c). In addition, for both Ni-LaCe 1:1 and Ni-LaCe 4:1 samples the Ni-

inclusion stabilized by the fiber channel and formation of a huge number of ordered layers of graphene are visible (insert in Fig.9 d). HR TEM images of spent catalysts after long run DRM are in good agreement with Raman and TGA data.

Conclusions

In the present work the effect of La/Ce atomic ratio (1:4; 1:1; 4:1) on the phase composition of the binary support and on the structure of Ni-containing catalysts was investigated before and after catalytic tests in DRM. For comparison Ni/CeO_2 was studied.

It was found that the nature of Ni-containing precursor formed over the support surface depends on the phase composition of the binary oxide. The formation of lanthanum nickelate phases was observed only for Ni-LaCe 4:1 sample, while for Ni-LaCe 1:1 and Ni-LaCe 1:4 samples the presence of $Ce_{0.46}La_{0.54}O_{2-\delta}$ and $Ce_{0.81}La_{0.19}O_{2-\delta}$ phases with fluorite structure promotes the formation of NiO strongly interacting with the support surface.

According with HRTEM results, Ni particles with sizes of up to 0.5 μm were found for the Ni-Ce sample. The addition of La to the support composition (La/Ce atomic ratio 1:4 and 1:1) significantly affected the sizes of Ni particles and their distribution over the binary La-Ce-O support surface. After reduction treatment, the particle size decreases (5-20 nm), their localization changed, mainly nanoparticles of active components are located at the grain boundaries of the supports. An increase in the content of La_2O_3 in the composition of the support in the case of a Ni-LaCe 4:1 catalyst leads to the decoration of small Ni NPs by lanthanum particles, which determines its low catalytic activity in the DRM reaction.

Acknowledgements

This work was supported by Russian Science Foundation (project 19-73-30026), except for BET, XRD, TGA and H_2-TPR studies that were supported by the Project PON (2015-2020) Energie per l'Ambiente – TARANTO ARS01_00637. The authors greatly acknowledge F. Giordano (ISMN-CNR, Italy) for XRD analyses.

References

[1] A. N. Şenera, M. E. Günay, A. Leba, R. Yıldırıma, Statistical review of dry reforming of methane literature using decision tree and artificial neural network analysis. Catal. Tod. 299 (2018) 289–302.

[2] C. Wang, Y. Wang, M. Chen, D. Liang, Z. Yang, W. Cheng, Z. Tang, J. Wang, H. Zhang, Recent adances during CH_4 dry reforming for syngas production: A mini review, Internat. J. Hydr. Energ. 46 (2021) 5852 – 5874.

[3] P. Frontera, A. Macario, A. Aloise, P. L. Antonucci, G. Giordano, J. B. Nagy, Effect of support surface on methane dry-reforming catalyst preparation, Catal. Tod. 218-219 (2013) 18-29.

[4] J.j. Huang, Y. Yan, S. Saqline, W. Liu, B. Liu, High performance Ni catalysts prepared by freeze drying for efficient dry reforming of methane Appl. Catal. B: Environ. 275 (2020) 119109.

[5] M. Akri, S. Zhao, X.Y. Li, K.T. Zang, A.F. Lee, Mark A. Isaacs, W. Xi, Y. Gangarajula, J. Luo, Y. Ren, Y.-T. Cui, L. Li, Y. Su, X. Pan, W. Wen, Y. Pan, K. Wilson, L. Li, B. Qiao, H. Ishii, Y.-F. Liao, A. Wang, X. Wang, T. Zhang, Atomically dispersed nickel as coke-resistant active sites for methane dry reforming. Nat Commun 10 (2019) article number 5181.

[6] M. Grabchenko, G. Pantaleo, F. Puleo, O. Vodyankina, L.F. Liotta, Ni/La_2O_3 catalysts for dry reforming of methane: Effect of La_2O_3 synthesis conditions on the structural properties and catalytic performances, Internat. J. Hydr. Energ. 46(11) (2021) 7939–7953.

[7] A. Löfberg, J. Guerrero-Caballero, T. Kane, A. Rubbens, L. Jalowiecki-Duhamel, Ni/CeO_2 based catalysts as oxygen vectors for the chemical looping dry reforming of methane for syngas production, Appl. Catal. B: Environ. 212 (2017) 159–174.

[8] I. Luisetto, S. Tuti, C. Romano, M. Boaro, E. Di Bartolomeo, J. Kopula Kesavan, S. Murugesan, S. Kumar, K. Selvakumare Dry reforming of methane over Ni supported on doped CeO_2: New insight on the role of dopants for CO_2 activation, J. CO_2 Utiliz. 30 (2019) 63-78.

[9] V. Rossato Bach, A. C. de Camargo, T. L. Souza, L. Cardozo-Filho, H. J. Alves, Dry reforming of methane over Ni/MgO–Al_2O_3 catalysts: Thermodynamic equilibrium analysis and experimental application, Internat. J. Hydr. Energ. 45(8) (2020) P. 5252-5263.

[10] Y. Lu, D. Guo, Y. Zhao, P.S. Moyo, Y. Zhao, S. Wang, X. Ma, Enhanced catalytic performance of Ni_x-V@HSS catalysts for the DRM reaction: The study of interfacial effects on Ni-VOx structure with a unique yolk-shell structure, J. Catal. 396 (2021) 65-80.

[11] M. Zhang, J. Zhang, Y. Wu, J. Pan, Q. Zhang, Y. Tan, Y. Han, Insight into the effects of the oxygen species over Ni/ZrO_2 catalyst surface on methane reforming with carbon dioxide, Appl. Catal. B: Environ. 244 (2019) 427-437.

[12] Liu, F., Zhao, L., Wang, H., Bai, X., and Liu, Y., Study on the preparation of Ni–La–Ce oxide catalyst for steam reforming of ethanol, Internat. J. Hydr. Energ. 39 (2014) 10454-10466.

[13] M. Makri, M. Vasiliades, K. Petallidou, A. Efstathiou, Effect of support composition on the origin and reactivity of carbon formed during dry reforming of methane over 5wt% Ni/$Ce_{1-x}M_xO_{2-\delta}$ (M = Zr^{4+}, Pr^{3+}) catalysts, Catal. Tod. 259 (2016) 150-164.

[14] A. Kambolis, H. Matralis, A. Trovarelli, C. Papadopoulou, Ni/CeO_2–ZrO_2 catalysts for the dry reforming of methane. Appl. Catal. A Gen. 377 (2010) 16–26.

[15] J. A. Montoya, E. Romero-Pascual, C. Gimon, P. Del Angel, A. Monzon, Methane reforming with CO_2 over Ni/ZrO_2–CeO_2 catalysts prepared by sol-gel. Catal. Tod. 63 (2000) 71–85.

[16] L. Li, B. S. Liu, J. W. H. Leung, C. T. Au, A. S.-C. Cheung, CH_4/CO_2 reforming over La_2NiO_4 and 10%NiO/CeO_2–La_2O_3 catalysts under the condition of supersonic jet expansion via cavity ring-down spectroscopic analysis, Catal. Tod. 131(1–4) (2008) 533-540.

[17] L. Pino, A. Vita, M. Laganà, V. Recupero. Hydrogen from biogas: Catalytic tri-reforming process with Ni/La-Ce-O mixed oxides, Appl. Catal. B: Environ. 148–149 (2014) 91-105.

[18] L. Pino, C. Italiano, A. Vita, M. Laganà, V. Recupero, $Ce_{0.70}La_{0.20}Ni_{0.10}O_{2-\delta}$ catalyst for methane dry reforming: Influence of reduction temperature on the catalytic activity and stability, Appl. Catal. B: Environ. 218 (2017) 779-792.

[19] G. Pantaleo, V. La Parola, F. Deganello, P. Calatozzo, R. Bal, A.M. Venezi. Synthesis and support composition effects on CH_4 partial oxidation over Ni–CeLa oxides, Appl. Catal. B: Environ. 164 (2015) 135–143.

[20] Seyed Mehdi Mousavi et al. Preparation of mesoporous nanocrystalline 10%Ni/$Ce_{1-x}Mn_xO_2$ catalysts for dry reforming reaction. Internat. J. Hydr. Energ. 42 (2017) 24776-24784.

[21] V. M. Gonzalez-Delacruz, F. Ternero, R. Pereñíguez, A. Caballero, J. P. Holgado, Study of nanostructured Ni/CeO_2 catalysts prepared by combustion synthesis in dry reforming of methane, Appl. Catal. A Gen. 384 (2010) 1–9.

[22] C. G. Rotaru, G. Postole, M. Florea, F. Matei-Rutkovska, V. I. Pârvulescu, P. Gelin, Dry reforming of methane on ceria prepared by modified precipitation route, Appl. Catal. A Gen. 494 (2015) 29–40.

[23] I. Luisetto, S. Tuti, E. Di Bartolomeo, Co and Ni supported on CeO_2 as selective bimetallic catalyst for dry reforming of methane, Internat. J. Hydr. Energ. 37 (2012) 15992–15999.

[24] T. Odedairo, J. Chen, Z. Zhu, Metal–support interface of a novel Ni–CeO_2 catalyst for dry reforming of methane, Catal. Commun. 31 (2013) 25–3.

[25] X. Du, D. Zhang, L. Shi, R. Gao, J. Zhang, Morphology Dependence of Catalytic Properties of Ni/CeO_2 Nanostructures for Carbon Dioxide Reforming of Methane, J. Phys. Chem. C 116 (2012) 10009–10016.

[26] V.M. Gonzalez-DelaCruz, J.P. Holgado, R. Pereniguez, A. Caballero, Morphology changes induced by strong metal–support interaction on a Ni–ceria catalytic system. J. Catal. 257 (2008) 307–314.

[27] A. Trovarelli. Catalytic properties of ceria and CeO_2-containing materials. Catal. Rev. 38(4) (1996) 439–520.

[28] C. De Leitenburg, A. Trovarelli, J. A. Kaspar. Temperature-programmed and transient kinetic study of CO_2 activation and methanation over CeO_2 supported noble metals. J. Catal. 166 (1997) 98–107.

[29] S. M. Lima, J. M. Assaf, M. A. Peña, J. L. G. Fierro, Structural features of $La_{1-x}Ce_xNiO_3$ mixed oxides and performance for the dry reforming of methane, Appl. Catal. A, 311 (2006) 94.

[30] M. C. J. Bradford, M. A. Vannice. The role of metal-support interactions in CO_2 reforming of CH_4. Catal. Tod. 50 (1999) 87–96.

[31] M.W. Barsoum, Fundamentals of Ceramics, CRC Press, 2002.

[32] J. Zamudio-García, J. M. Porras-Vazquez, J. Canales-Vazquez, A. Cabeza, E. R. Losilla, D. Marrero-Lopez, Relationship between the Structure and Transport Properties in the $Ce_{1-x}La_xO_{2-x/2}$ System, Inorg. Chem. 58 (2019) 9368−9377.

[33] V.S. Urusov, Geometric model for deviations from Vegard's law // Journal of Structural Chemistry 33 (1992) 68–79.

[34] M. F. Wilkes, P. Hayden, A.K. Bhattacharya, Catalytic studies on ceria lanthana solid solutions III. Surface segregation and solid state studies. J. Catal. 219 (2003) 305-309.

[35] M. F. Wilkes, P. Hayden, A.K. Bhattacharya, Surface segregation of lanthanum and cerium ions in ceria/lanthana solid solutions: comparison between experimental results and a statistical-mechanical model. Appl. Surf. Sci. 206 (2003) 12-19.

[36] V. Belliere, G. Joorst, O. Stephan, F. M. F. de Groot, B. M. Weckhuysen, Phase Segregation in Cerium-Lanthanum Solid Solutions, J. Phys. Chem. B 110 (2006) 9984-9990.

[37] H.V Fajardo, L.F Probst, N.L Carreno, I.T Garcia, A. Valentini, Hydrogen production from ethanol steam reforming over Ni/CeO_2 nanocomposite catalysts. Catal Lett 119 (2007) 228-236.

[38] Sun, C., Beaunier, P., La Parola, V., Liotta, L.F., Da Costa, P. Ni/CeO_2Nanoparticles Promoted by Yttrium Doping as Catalysts for CO_2Methanation ACS Applied Nano Materials, 3 (12) (2020) 12355-12368.

[39] F.M.Z. Zotin, L. Tournayan, J. Varloud, V. Perrichon, R. Fréty, Temperature-programmed reduction: limitation of the technique for determining the extent of reduction of either pure ceria or ceria modified by additive. Appl. Catal. A: Gen. 98 (1993) 99-114.

[40] Mirosław Szybowicz, Ariadna B. Nowicka and Anna Dychalska // Characterization of Carbon Nanomaterials by Raman Spectroscopy Chapter 1 in Characterization of Nanomaterials 2018 Elsevier Ltd.

[41] N.D. Charisiou, L. Tzounis, V. Sebastian, S.J. Hindere, M.A. Baker, K. Polychronopoulou , M.A. Goula Investigating the correlation between deactivation and the carbon deposited on the surface of Ni/Al_2O_3 and Ni/La_2O_3-Al_2O_3 catalysts during the biogas reforming reaction. Appl. Surf. Science 474 (2018) 42-56.

Table 1 – Crystalline phase parameters for the air-calcined supports.

Sample	a, A	Space Group	Solid solution composition	D^*_{XRD}, nm	$\Delta d/d \cdot 10^3$*
Ce	5.41	Fm3hm	$CeO_{2-\delta}$	55	0.5
LaCe 1:4	5.47	Fm3hm	$Ce_{0.81}La_{0.19}O_{2-\delta}$	24	1.9
LaCe 1:1	5.58	Fm3hm	$Ce_{0.46}La_{0.54}O_{2-\delta}$	27	2.9
LaCe 4:1	11.73	Ia3	n.d.	25	3.3

*Crystallite size (D) and microstrain ($\Delta d/d$)

Table 2 – Crystalline phase parameters for the air-calcined Ni-containing catalysts

Sample	$Ce_{1-x-y}La_xNi_yO_{2-\delta}$				Ni-containing phase		
	a, A	Space Group	D_{XRD}, nm	$\Delta d/d \cdot 10^3$	Phase	D_{XRD}, nm	$\Delta d/d \cdot 10^3$
Ni-Ce	5.41	Fm3hm	54	0.6	NiO	65	0.5
Ni-LaCe1:4	5.47	Fm3hm	25	1.0	NiO	13	1.8
Ni-LaCe 1:1	5.57	Fm3hm	27	2.9	NiO	15	1.9
Ni-LaCe 4:1	5.74/11.50	Fm3hm/Ia3	20	1.7	$LaNiO_3$, La_2NiO_4, NiO (traces)	n.d.	n.d

Table 3.

Samples	T_{max} (°C)	Experimental H_2 consumptions (mL/g)	Reactions	Theoretical H_2 consumptions (mL/g)
Ni-Ce	327	40.1	$Ni^{2+} \rightarrow Ni^0$ Ce^{4+}(surf.)$\rightarrow Ce^{3+}$	41.7 ($Ni^{2+/0}$) 63.9 ($Ce^{4+/3+}$)*
	850	23.1	Ce^{4+} (bulk)$\rightarrow Ce^{3+}$	
Total consumption (mL H_2/g)		63.2		77.7
Ni-LaCe 1:4	392	48.0	$Ni^{2+} \rightarrow Ni^0$ $Ce^{4+} \rightarrow Ce^{3+}$	41.7 ($Ni^{2+/0}$) 52.7 ($Ce^{4+/3+}$)
Total consumption (mL H_2/g)		48.0		68.5
Ni-LaCe 1:1	352	42.5	$Ni^{2+} \rightarrow Ni^0$ $Ce^{4+} \rightarrow Ce^{3+}$	41.7 ($Ni^{2+/0}$) 33.2 ($Ce^{4+/3+}$)
Total consumption (mL H_2/g)		42.5		59.7
Ni-LaCe 4:1	350 520	27.6 15.7	$Ni^{2+} \rightarrow Ni^0$ $Ce^{4+} \rightarrow Ce^{3+}$	41.7 ($Ni^{2+/0}$) 21.5 ($Ce^{4+/3+}$)
Total consumption (mL H_2/g)		43.3		54.9

*The theoretical hydrogen consumption for ceria was calculated on the hypothesis of an overall reduction $Ce^{4+} \rightarrow Ce^{3+}$, but this not achievable in the TPR conditions herein used [39].

Table 4 – Crystalline phase parameters for the reduced Ni-containing catalysts.

Sample	$Ce_{1-x}La_xO_{2-\delta}$				Ni	
	a, A	Space Group	D_{XRD}, nm	$\Delta d/d \cdot 10^3$	D_{XRD}, nm	$\Delta d/d \cdot 10^3$
Ni-Ce	5.41	Fm3hm	61	0.6	78	0.5
Ni-LaCe 1:4	5.47	Fm3hm	26	0.9	10	5.7
Ni-LaCe 1:1	5.57	Fm3hm	22	1.1	26	1.9
Ni-LaCe 4:1	5.65/11.29	Fm3hm/Ia3	18	1.9	n.d.	n.d.

Table 5 – Crystalline phase parameters for the Ni-containing catalysts after DRM.

Sample	$Ce_{1-x}La_xO_{2-\delta}$				Ni	
	a, A	Space Group	D_{XRD}, nm	$\Delta d/d \cdot 10^3$	D_{XRD}, nm	$\Delta d/d \cdot 10^3$
Ni-Ce	5.41	Fm3hm	76	0.5	84	0.5
Ni-LaCe 1:4	5.47	Fm3hm	29	0.9	20	1.9
Ni-LaCe 1:1	5.57	Fm3hm	26	1.3	30	1.6
Ni-LaCe 4:1	5.67/11.31	Fm3hm/Ia3	16	2.1	n.d.	n.d.

Supporting Information

Supplementary Tables

Table S1. Textural properties of the prepared catalysts

Sample	S_{BET} (m^2/g)	Pore volume (cm^3/g)	Average pore size (nm)
Ni-Ce	13.1	0.08	15.0
NiLaCe 1:4	12.2	0.07	13.8
Ni-LaCe 1:1	11.4	0.06	11.2
Ni-LaCe 4:1	10.8	0.055	9.3

Table S2. Main catalytic results during DRM tests (gradient temperature and long run (LR) tests) carried out over prepared catalysts.

Sample	**Parameter**	**650°C**	**700°C**	**800°C**	**Start LR 650°C**	**End LR 650°C**
Ni-Ce	Conv. CO_2 (%)	50.5	67.3	91.5	49.0	43.4
	Conv. CH_4 (%)	36.1	52.6	81.4	34.8	30.0
	H_2 Yield (%)	21.5	33.8	57.2	20.7	17.3
	H_2/CO	0.55	0.65	0.73	0.55	0.53
Ni-LaCe 1:4	Conv. CO_2 (%)	65.9	82.3	97.6	65.8	63.6
	Conv. CH_4 (%)	51.5	70.1	92.8	51.5	49.0
	H_2 Yield (%)	30.5	45.1	63.8	30.5	28.7
	H_2/CO	0.64	0.74	0.88	0.64	0.63
Ni-LaCe 1:1	Conv. CO_2 (%)	65.2	80.8	95.3	64.0	61.3
	Conv. CH_4 (%)	52.1	71.2	92.7	51.0	48.0
	H_2 Yield (%)	33.1	48.2	66.2	32.4	29.7
	H_2/CO	0.67	0.78	0.89	0.66	0.64
Ni-LaCe 4:1	Conv. CO_2 (%)	40.4%	74.0	96.5	39.3	42.4
	Conv. CH_4 (%)	25.7%	60.0	93.9	24.6	27.4
	H_2 Yield (%)	14.1%	39.9	68.2	13.4	15.6
	H_2/CO	0.45	0.69	0.9	0.45	0.48

Captions

Fig. 1. XRD patterns of the calcined supports (a) and Ni catalysts (b)

Fig. 2. H_2-TPR profiles of the calcined catalysts.

Fig. 3. XRD patterns of the reduced nickel catalysts.

Fig. 4. CO_2 and CH_4 conversion values (a, b) and H_2 yield (open symbols) and H_2/CO ratio (filled symbols) versus temperature (c) for Ni-containing catalysts during DRM at gradient temperature.

Fig. 5. DRM long run tests at 650 °C during 24 h for Ni-containing catalysts.

Fig. 6 XRD patterns of catalysts after long run DRM test.

Fig.7. TGA curves of catalysts in and airflow after long run DRM test.

Fig. 8. Raman spectra of the spent catalysts after long run DRM test.

Fig. 9. TEM HR images of carbon formation after DRM reaction for Ni-Ce (a), Ni-LaCe 1:4 (b), Ni-LaCe 1:1 (c), Ni-LaCe 4:1 (d).

Fig. S1. HAADF image (a) of reduced Ni-Ce sample with the corresponding Ce and Ni mapping distribution (b).

Fig. S2. HAADF image (a) of reduced Ni-LaCe 1:4 sample with the corresponding La and Ni mapping distribution (b).

Fig. S3. TEM (a) and TEM HR (b) images of reduced Ni-LaCe 1:1 the corresponding Ni mapping distribution (c).

Fig. S4. TEM image (a) and HAADF image of Ni-LaCe 4:1 catalyst (b) with corresponding Ni mapping distribution (c).

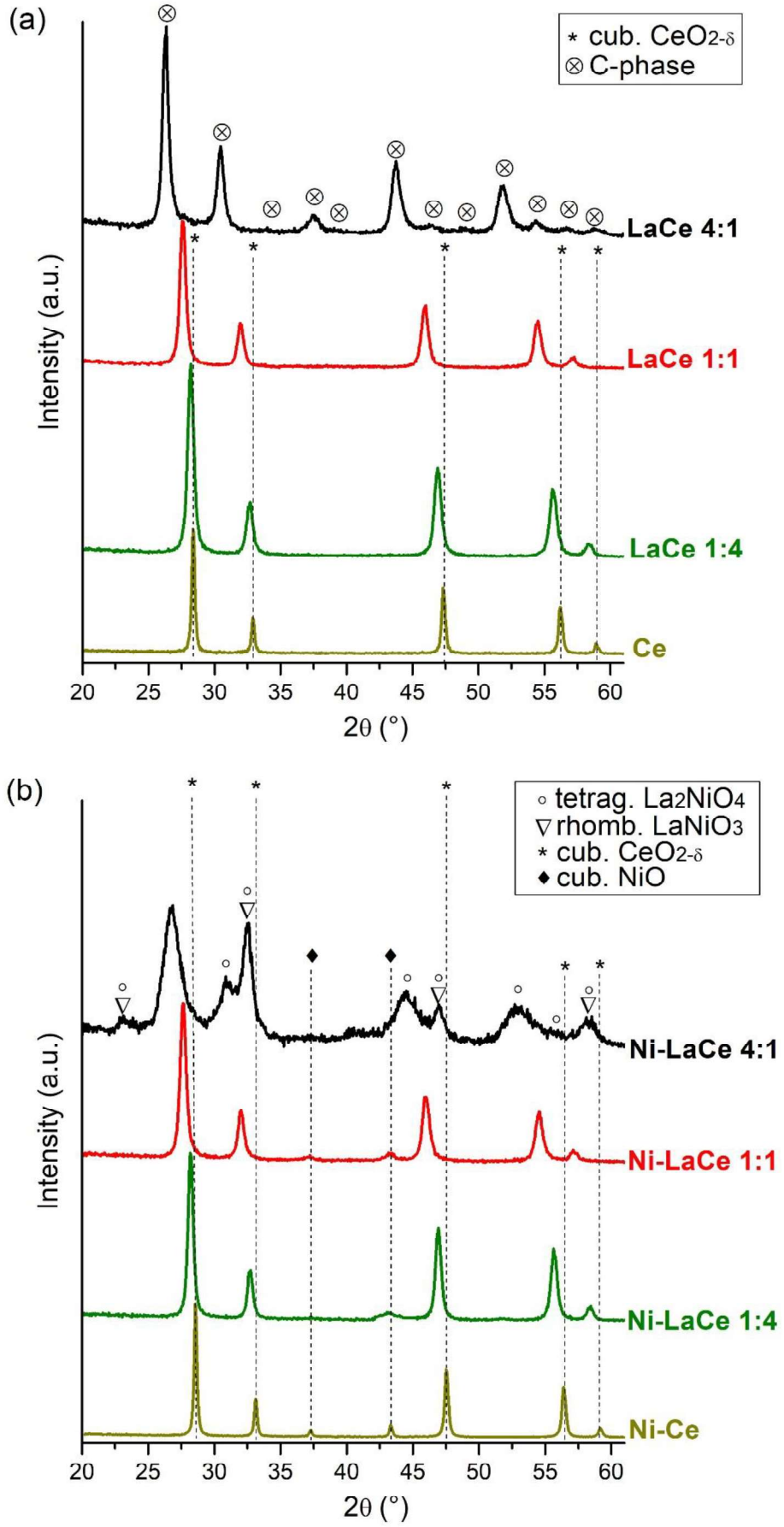
(a)
* cub. CeO2-δ
⊗ C-phase
LaCe 4:1
LaCe 1:1
LaCe 1:4
Ce
Intensity (a.u.)
20 25 30 35 40 45 50 55 60
2θ (°)
(b)
○ tetrag. La2NiO4
▽ rhomb. LaNiO3
* cub. CeO2-δ
◆ cub. NiO
Ni-LaCe 4:1
Ni-LaCe 1:1
Ni-LaCe 1:4
Ni-Ce
Intensity (a.u.)
20 25 30 35 40 45 50 55 60
2θ (°)

Fig. 1.

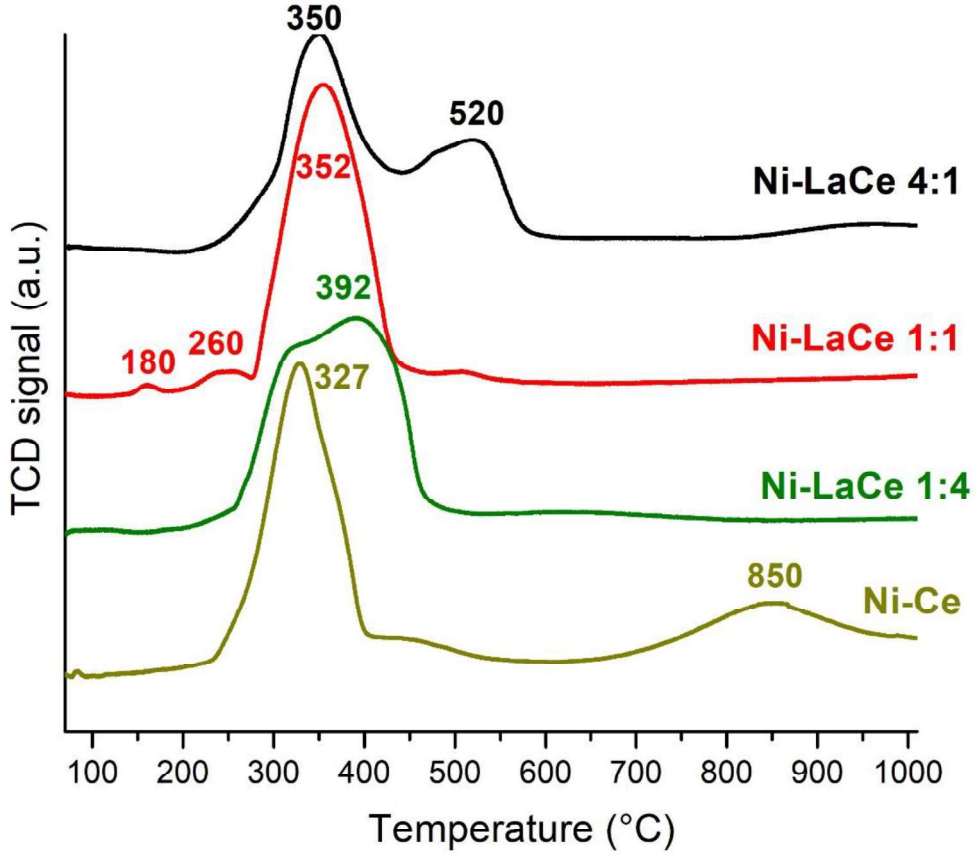
350
520
352
Ni-LaCe 4:1
392
180
260
Ni-LaCe 1:1
327
Ni-LaCe 1:4
850
Ni-Ce
TCD signal (a.u.)
100
200
300
400
500
600
700
800
900
1000
Temperature (°C)

Fig. 2.

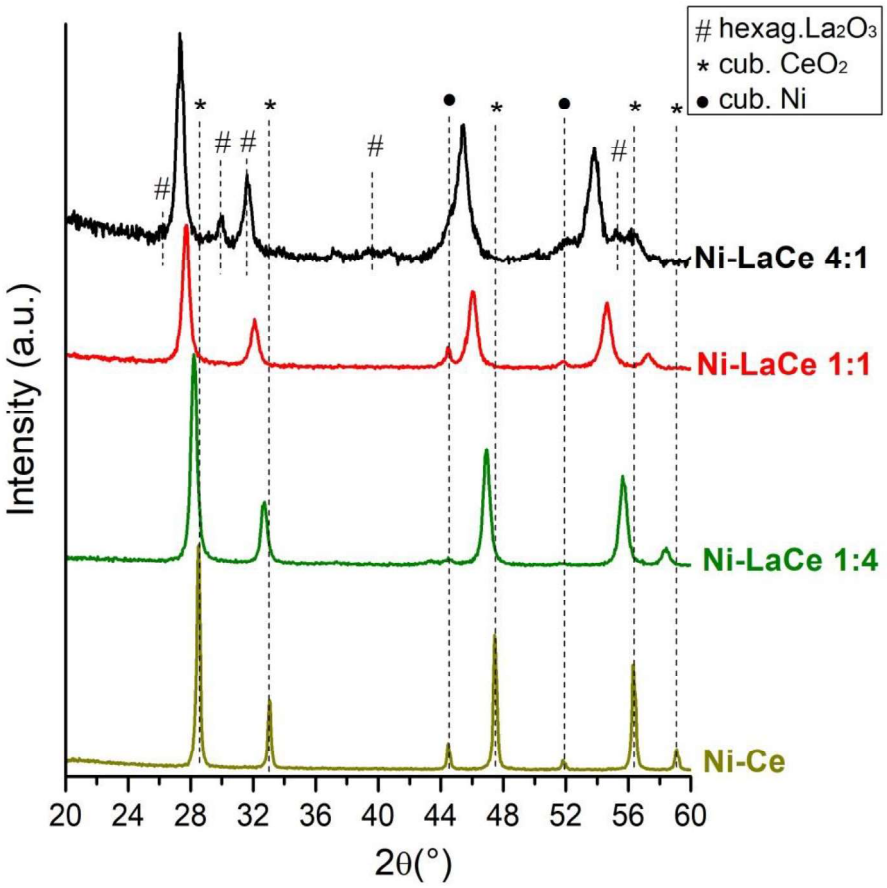
hexag.La2O3
* cub. CeO2
● cub. Ni
Ni-LaCe 4:1
Ni-LaCe 1:1
Ni-LaCe 1:4
Ni-Ce
Intensity (a.u.)
20 24 28 32 36 40 44 48 52 56 60
2θ(°)

Fig. 3.

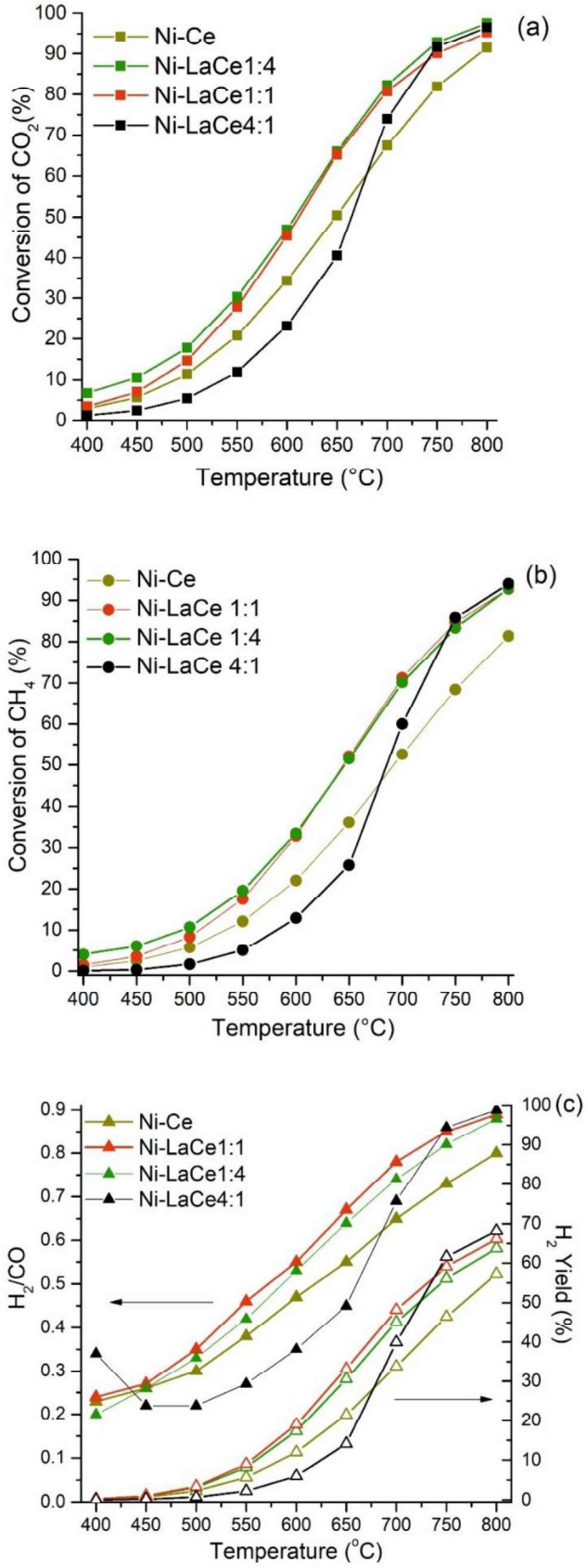
(a)
Ni-Ce
Ni-LaCe1:4
Ni-LaCe1:1
Ni-LaCe4:1
Conversion of CO_2(%)
Temperature (°C)
(b)
Ni-Ce
Ni-LaCe 1:1
Ni-LaCe 1:4
Ni-LaCe 4:1
Conversion of CH_4 (%)
Temperature (°C)
(c)
Ni-Ce
Ni-LaCe1:1
Ni-LaCe1:4
Ni-LaCe4:1
H_2/CO
H_2 Yield (%)
Temperature (°C)

Fig. 4.

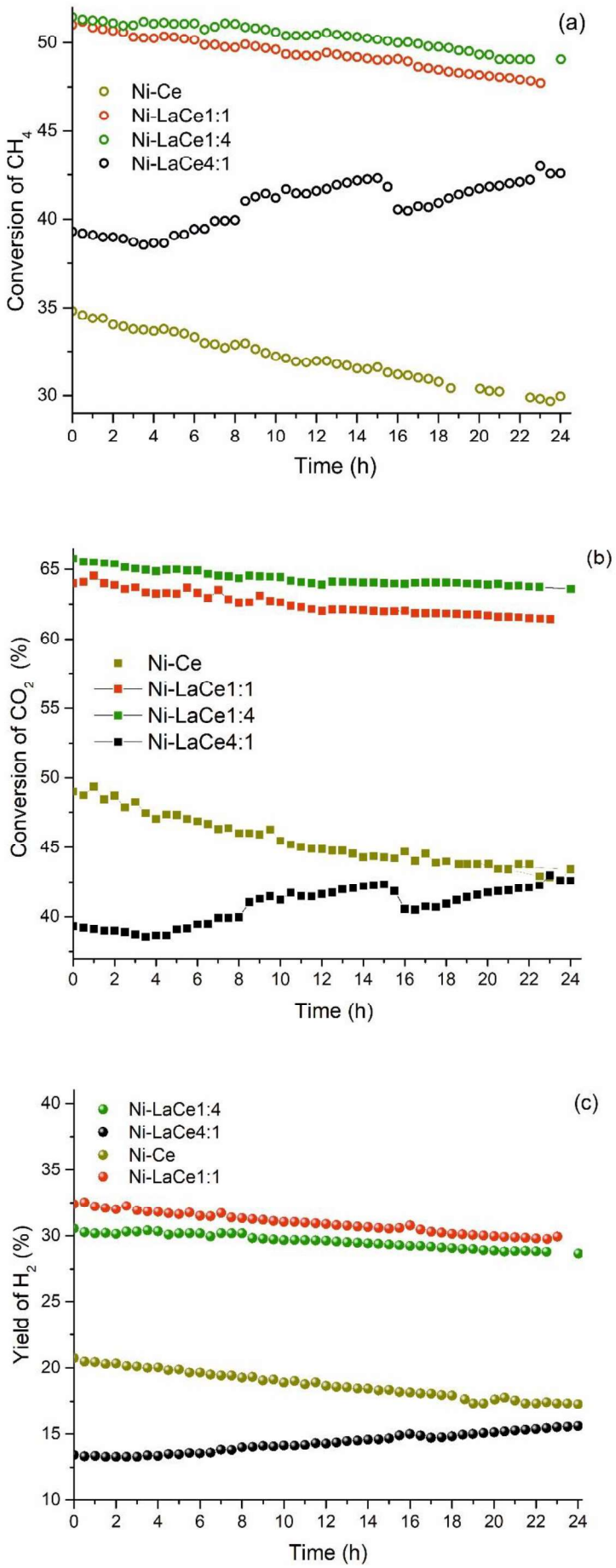
(a)
Ni-Ce
Ni-LaCe1:1
Ni-LaCe1:4
Ni-LaCe4:1
Conversion of CH4
Time (h)
(b)
Ni-Ce
Ni-LaCe1:1
Ni-LaCe1:4
Ni-LaCe4:1
Conversion of CO2 (%)
Time (h)
(c)
Ni-LaCe1:4
Ni-LaCe4:1
Ni-Ce
Ni-LaCe1:1
Yield of H2 (%)
Time (h)

Fig. 5.

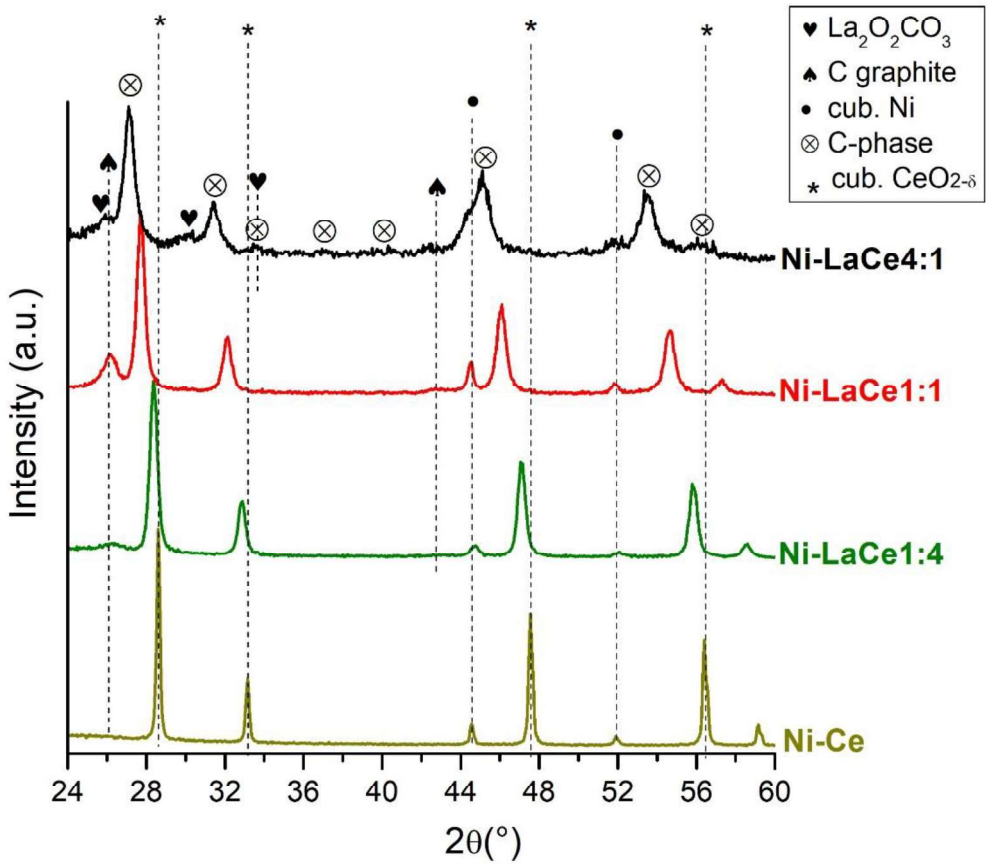
♥ La2O2CO3
♠ C graphite
• cub. Ni
⊗ C-phase
* cub. CeO2-δ
Ni-LaCe4:1
Ni-LaCe1:1
Ni-LaCe1:4
Ni-Ce
Intensity (a.u.)
24
28
32
36
40
44
48
52
56
60
2θ(°)

Fig. 6.

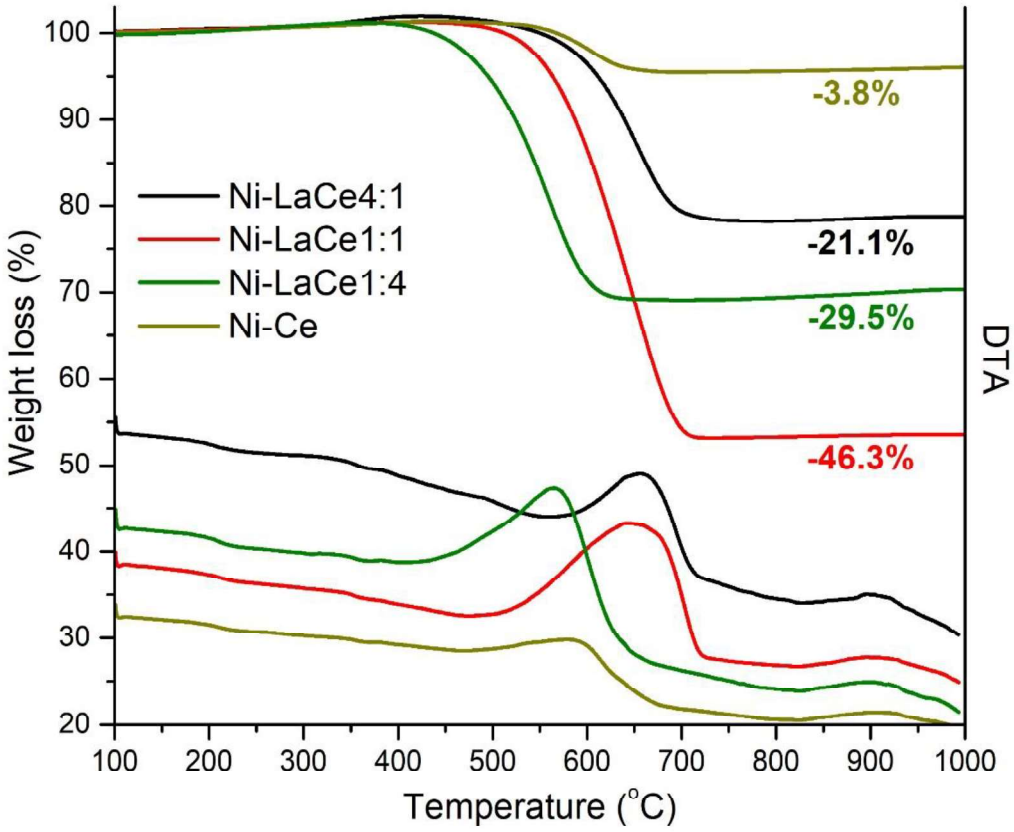
Weight loss (%)
Temperature (°C)
DTA
Ni-LaCe4:1
Ni-LaCe1:1
Ni-LaCe1:4
Ni-Ce
-3.8%
-21.1%
-29.5%
-46.3%
100
90
80
70
60
50
40
30
20
100
200
300
400
500
600
700
800
900
1000

Fig. 7.

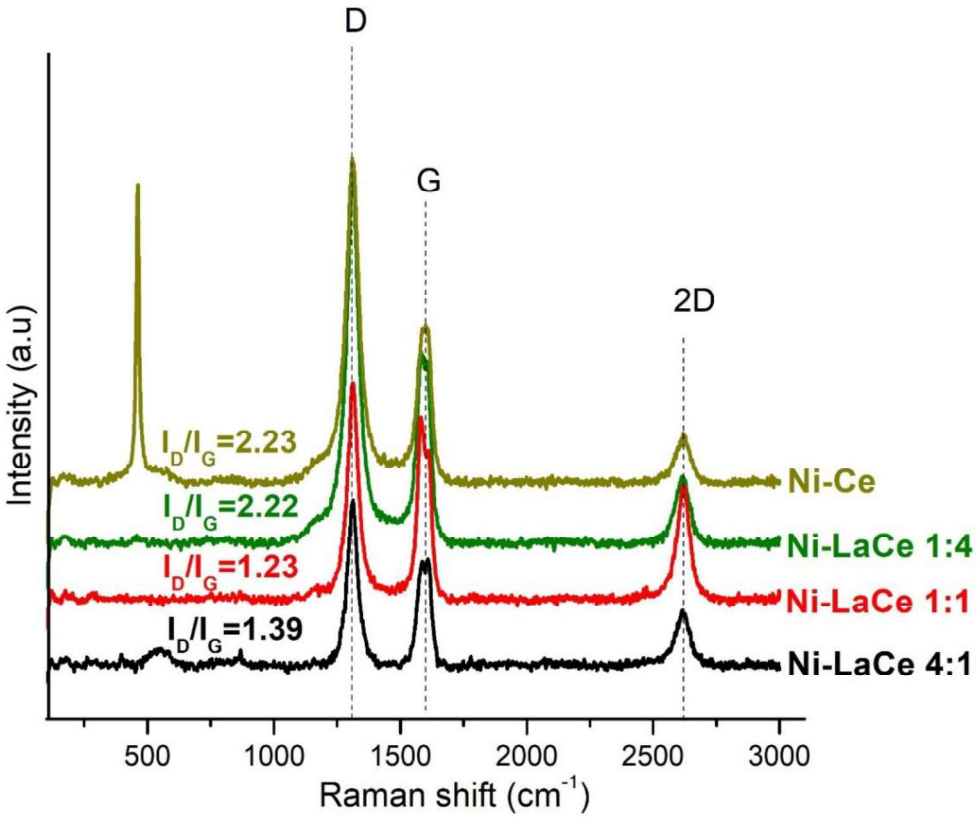
D
G
2D
Intensity (a.u)
I_D/I_G=2.23
I_D/I_G=2.22
I_D/I_G=1.23
I_D/I_G=1.39
Ni-Ce
Ni-LaCe 1:4
Ni-LaCe 1:1
Ni-LaCe 4:1
500
1000
1500
2000
2500
3000
Raman shift (cm^{-1})

Fig. 8.

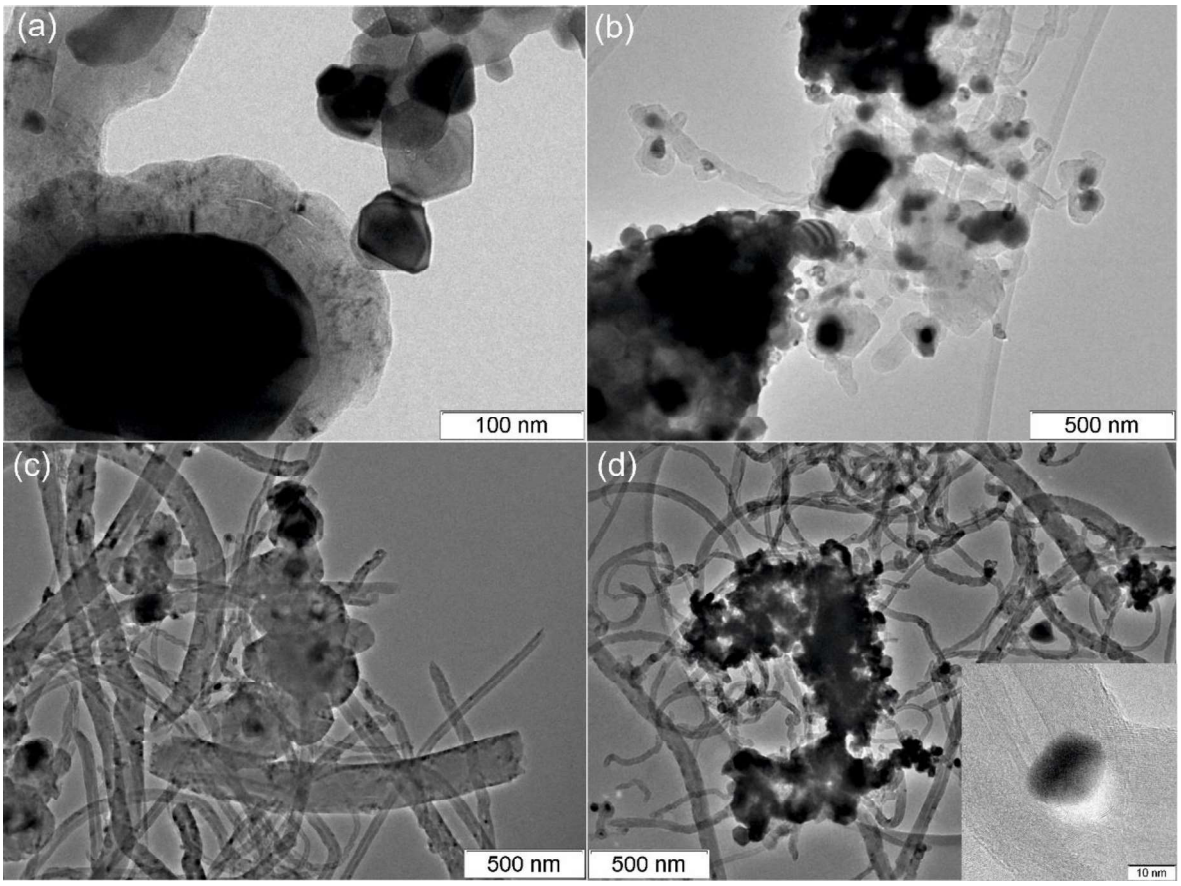

Fig. 9.

Supporting information

Supplementary Figures

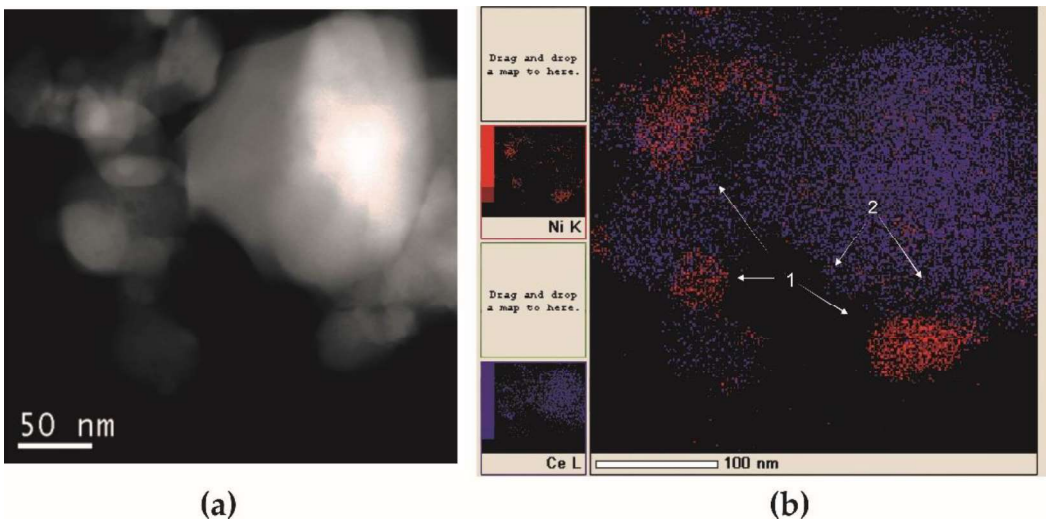

Fig. S1. HAADF image (a) of reduced Ni-Ce sample with the corresponding Ce and Ni mapping distribution (b).

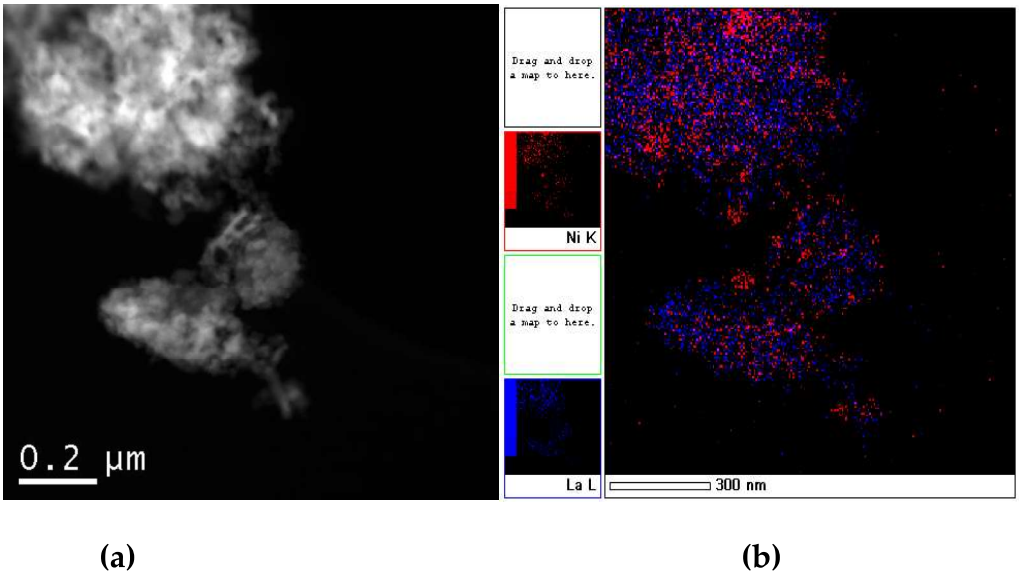

Fig. S2. HAADF image (a) of reduced Ni-LaCe 1:4 sample with the corresponding La and Ni mapping distribution (b).

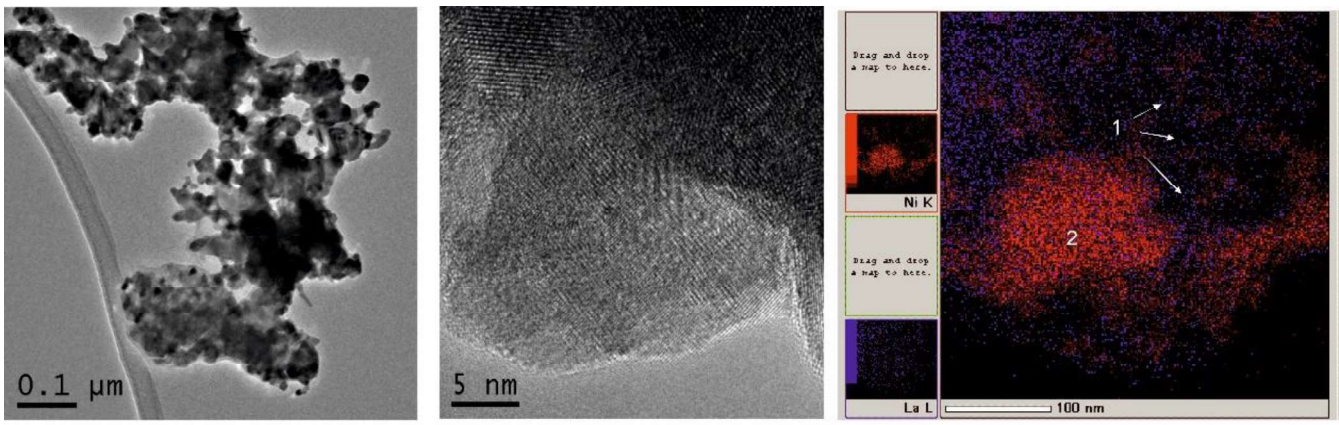

(a) (b) (c)

Fig. S3. TEM (a) and TEM HR (b) images of reduced Ni-LaCe 1:1 the corresponding Ni mapping distribution (c).

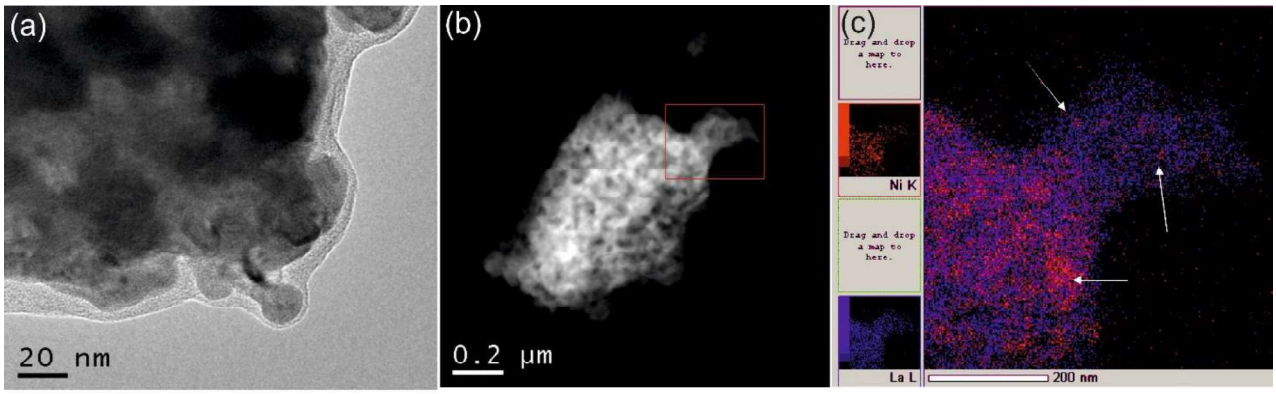

Fig. S4. TEM image (a) and HAADF image of Ni-LaCe 4:1 catalyst (b) with corresponding Ni mapping distribution (c).

Credit Author Statement

AUTHORSHIP STATEMENT

Manuscript title: Design of Ni-based catalysts supported over binary La-Ce oxides: Influence of La/Ce ratio on the catalytic performances in DRM.

All persons who meet authorship criteria are listed as authors, and all authors certify that they have participated sufficiently in the work to take public responsibility for the content, including participation in the concept, design, analysis, writing, or revision of the manuscript. Furthermore, each author certifies that this material or similar material has not been and will not be submitted to or published in any other publication before its appearance in the *Hong Kong Journal of Occupational Therapy*.

Authorship contributions

Please indicate the specific contributions made by each author (list the authors' initials followed by their surnames, e.g., Y.L. Cheung). The name of each author must appear at least once in each of the three categories below.

Category 1

Conception and design of study: L.F. Liotta, O.V. Vodyankina, _____;

acquisition of data: G. Pantaleo, F. Puleo, M. Grabchenko, V.I. Zaikovskii

analysis and/or interpretation of data: M. Grabchenko, T.S. Kharlamova, V.I. Zaikovskii

Category 2

Drafting the manuscript: M. Grabchenko, L.F. Liotta, T.S. Kharlamova;

revising the manuscript critically for important intellectual content: M. Grabchenko, T.S. Kharlamova, O.V. Vodyankina, L.F. Liotta.

Category 3

Approval of the version of the manuscript to be published (the names of all authors must be listed):

M. Grabchenko, G. Pantaleo, F. Puleo, T.S. Kharlamova, V.I. Zaikovskii

O. Vodyankina, L.F. Liotta, _____, _____, _____.

Acknowledgements

All persons who have made substantial contributions to the work reported in the manuscript (e.g., technical help, writing and editing assistance, general support), but who do not meet the criteria for authorship, are named in the Acknowledgements and have given us their written permission to be named. If we have not included an Acknowledgements, then that indicates that we have not received substantial contributions from non-authors.

This statement is signed by all the authors (*a photocopy of this form may be used if there are more than 10 authors*):

Author's name (typed)	Author's signature	Date
M. Grabchenko		29.06.2021
G. Pantaleo	Giuseppe Pantaleo	30.06.2021
F. Puleo	Fabrizio Puleo	30.06.2021
T.S. Kharlamova		29.06.2021
V.I. Zaikovskii		29.06.2021
O. Vodyankina		29.06.2021
L.F. Liotta	Leonarda F. Liotta	30.06.2021

Declaration of interests

☒ The authors declare that they have no known competing financial interests or personal relationships that could have appeared to influence the work reported in this paper.

☐The authors declare the following financial interests/personal relationships which may be considered as potential competing interests:

I'm signing on behalf of all the co-authors

Sincerely yours

Dr.ssa LF Liotta

Leonarda Liotta

CONSIGLIO NAZIONALE DELLE RICERCHE I.S.M.N. PALERMO